

Original Article

Cite this article: Prakash D, Patel DK, Yadav MK, Vishal B, Tewari S, Yadav R, Rai SK, and Singh CK (2020) Prograde polyphase regional metamorphism of pelitic rocks, NW of Jamshedpur, eastern India: constraints from textural relationship, pseudosection modelling and geothermobarometry. *Geological Magazine* 157: 1045–1067. <https://doi.org/10.1017/S0016756819001171>

Received: 1 February 2019

Revised: 14 July 2019

Accepted: 27 August 2019

First published online: 11 November 2019



Keywords:

prograde Barrovian metamorphism; textural relationship; pseudosection modelling; geothermobarometry; eastern India

Author for correspondence:

DK Patel, Email: dkpbhugueo@gmail.com

Prograde polyphase regional metamorphism of pelitic rocks, NW of Jamshedpur, eastern India: constraints from textural relationship, pseudosection modelling and geothermobarometry

D Prakash¹ , DK Patel¹ , MK Yadav², B Vishal¹, S Tewari³, R Yadav¹, SK Rai¹ and CK Singh¹

¹Centre of Advanced Study in Geology, Banaras Hindu University, Varanasi 221005, India; ²Centre of Advanced Study in Geology, University of Lucknow, Lucknow 226007, India and ³Centre for Earth Sciences, Indian Institute of Science, Bangalore 560012, India

Abstract

The study area belongs to the Singhbhum metamorphic belt of Jharkhand, situated in the eastern part of India. The spatial distribution of the index minerals in the pelitic schists of the area shows Barrovian type of metamorphism. Three isograds, viz. garnet, staurolite and sillimanite, have been delineated and the textural study of the schists has revealed a time relation between crystallization and deformation. Series of folds with shifting values of plunges in the supracrustal rocks having axial-planar schistosity to the folds have been widely cited. Development of these folds could be attributed to the second phase of deformation. In total, two phases of deformation, D₁ and D₂, in association with two phases of metamorphism, M₁ and M₂, have been lined up in the study area. Chemographic plots of reactant and product assemblages corresponding to various metamorphic reactions suggest that the pattern of metamorphic zones mapped in space is in coherence with the temporal-sequential change during prograde metamorphism. The prograde *P–T* evolution of the study area has been obtained using conventional geothermobarometry, internally consistent winTWQ program and Perple_X software in the MnNCKFMASHTO model system. Our observations suggest that the progressive metamorphism in the area is not related to granitic intrusion or migmatization but that it was possibly the ascending plume that resulted in the M₁ phase of metamorphism followed by D₁ deformation. The second and prime metamorphic phase, M₂, with its possible heat source generated by crustal overloading, was preceded by D₁ and it lasted until late- to post-D₂ deformation.

1. Introduction

The Singhbhum Craton (SC) of India is separated from the Chhotanagpur Gneissic Complex (CGC) in the north by the Tamar–Porapahar shear zone, and in the south it is separated from the Eastern Ghats Mobile Belt (EGMB) by the Sukinda shear zone. The North Singhbhum Mobile Belt (NSMB) is the part of the Central Indian Suture Zone (CISZ), situated north of the Singhbhum Archaean centre (Mukhopadhyay, 2001) and comprises metamorphosed rocks of varying protoliths such as volcanoclastic, siliciclastic and pelitic compositions (Sarkar & Saha, 1962). The NSMB is part of the Older Metamorphic Group (OMG) of peninsular India. The OMG as a supracrustal must have been initially deposited as sediments and volcanics on an earlier basement, now unidentifiable in the region. The transformation and remobilization of initially deposited sediments and volcanics generating granitic rocks might have been the major cause of their non-recognizable nature. In addition, there are also evidences of several later-generation granites that are now grouped in the Singhbhum Granite Complex (SGC). The study area, Kandra (22° 47' to 22° 55' N, 86° 00' to 86° 05' E; Fig. 1a, b) lies c. 20 km NW of Jamshedpur city, Jharkhand, and is characterized by a well-developed Barrovian facies series. It includes rock types such as mica schist, amphibolites, and quartzites, etc. These rocks are of Proterozoic age and represent a part of Singhbhum Orogeny (Saha, 1970; Matin *et al.* 2012; Banerjee & Matin, 2013). Previously, different aspects of the geology of this area have been described by various workers (Dunn & Dey, 1942; Mitra, 1954; Roy, 1966; Chakraborty & Sen, 1967; Lal & Singh, 1978; Lal *et al.* 1987; Dwivedi & Lal, 1992; Dwivedi *et al.* 1993). Based on the first appearance of the index minerals, this area may be divided into four metamorphic zones: (1) biotite zone, (2) garnet zone, (3) staurolite zone, (4) sillimanite zone (Prakash *et al.* 2017). In this metamorphic belt, kyanite appears much earlier than staurolite and it occurs sporadically in staurolite schists. Hence, it is not possible to demarcate kyanite isograd separately on the

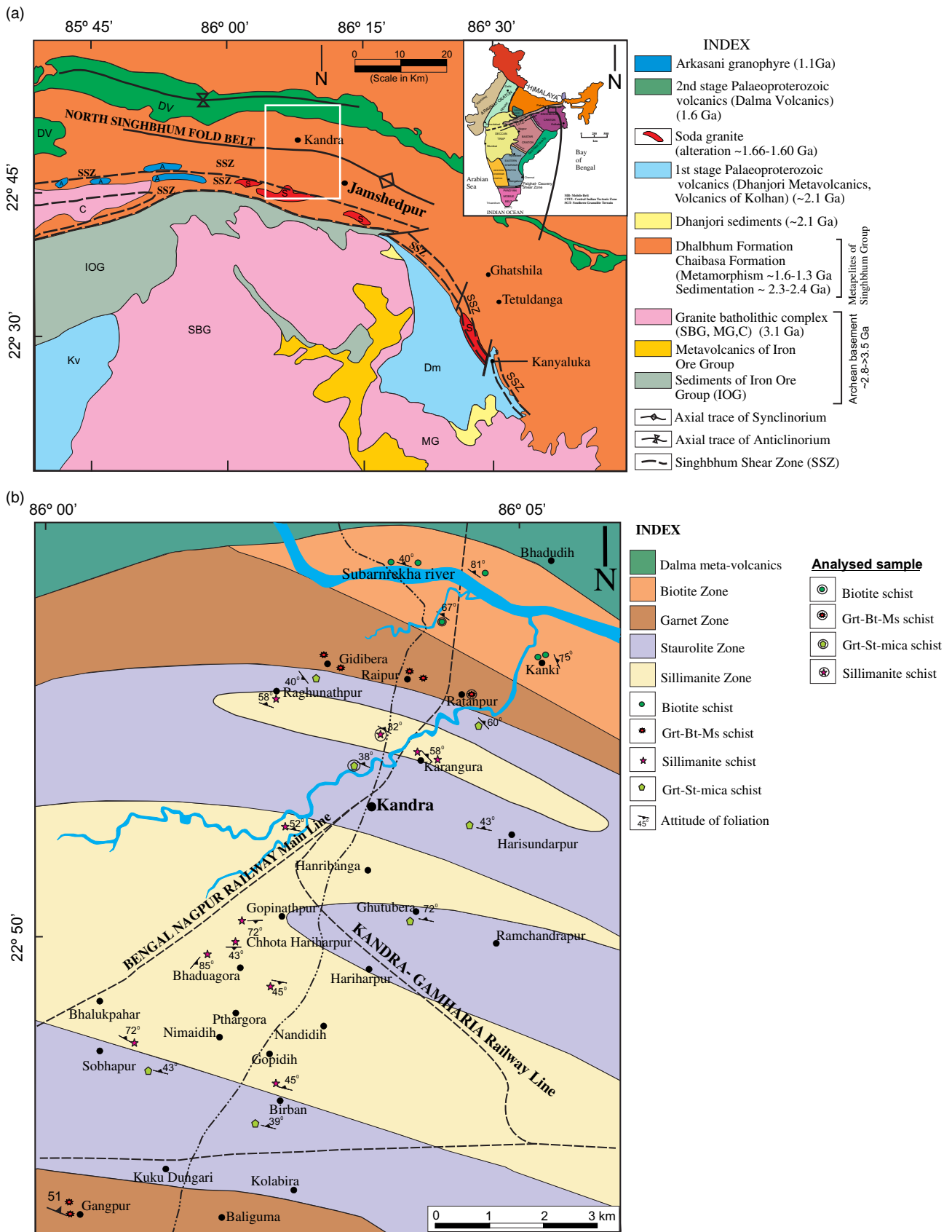


Fig. 1. (Colour online) (a) Simplified geological map of Singhbhum craton showing the main lithological units and structural elements as well as the location of the study area (modified after Chakraborty et al. 2015). The area marked by the box is elaborated in (b); SBG, Singhbhum Granite; MG, Mayurbhanj Granite; C, Chakradharpur Granite; Dm, Dhanjori Metavolcanics; Kv, Volcanics of Kolhan Group; S, Soda Granite; DV, Dalma Volcanics; A, Arkasani Granophyre. (b) Geological map of the study area delineated into different zones and isograds (modified after Prakash et al. 2017).

Table 1. Generalized lithological and chronological events in the North Singhbhum Fold Belt (NSFB) and Singhbhum Shear Zone (SSZ) (modified after Chakraborty *et al.* 2015)

Unit	Lithology	Metamorphism	Age
Chandil Formation	Rhyolite, tuff, agglomerates, shale, C-shale	Low greenschist (phyllite)	Thermal event: $\sim 1.5 \text{ Ga}^8$ Rhyolite emplacement: $\sim 1.63 \text{ Ga}^7$
Dalma Formation	Basic lava and volcano-clastic sediments of continental affinity	Greenschist	Metamorphism (?): 1.6 Ga^6
Dhalbhum Formation	Sandstone, siltstone, orthoquartzite, shale, tuff of continental affinity	Greenschist	Unknown
SSZ melange	Chlorite quartz schist, talc/actinolite schist, magnetite-apatite rock, Cu-U ores, tourmalinite, kyanite-bearing quartzite, chloritoid schist, etc.	Greenschist to amphibolite	Shearing and hydrothermal alteration: $1.66\text{--}1.60 \text{ Ga}^5$ and $\sim 1.0 \text{ Ga}^5$ Protolith formation: $\sim 1.9\text{--}1.8 \text{ Ga}^5$
Soda granite (only in SSZ)	Granitoids	Greenschist to amphibolite hydrothermally altered	Hydrothermal alteration: $\sim 1.66\text{--}1.60 \text{ Ga}^5$ Emplacement: $\sim 2.2 \text{ Ga}^4$
Chaibasa Formation	Shale, sandstone, and orthoquartzite with minor basic to ultrabasic rocks of marine affinity	Greenschist to amphibolite	Metamorphism: $\sim 1.6\text{--}1.3 \text{ Ga}^3$
Dhanjhour Formation	Basic and dacitic lavas, quartzite minor shale, and basal conglomerate of continental affinity		Lava flow: $\sim 2.1 \text{ Ga}^2$
Archaean basement	Unconformity – metasedimentary rocks, tonalite, trondjemite and granitoids intrusions		$\sim 2.8\text{--}3.5 \text{ Ga}^1$

Notes: Reviewed in ¹Mazumder *et al.* (2012a, b), ²Roy *et al.* (2002b), ³Mahato *et al.* (2008), ⁴Sarkar *et al.* (1985), ⁵Pal and Rhede (2013), ⁶Roy *et al.* (2002a), ⁷Reddy *et al.* (2009), ⁸Sengupta *et al.* (2000).

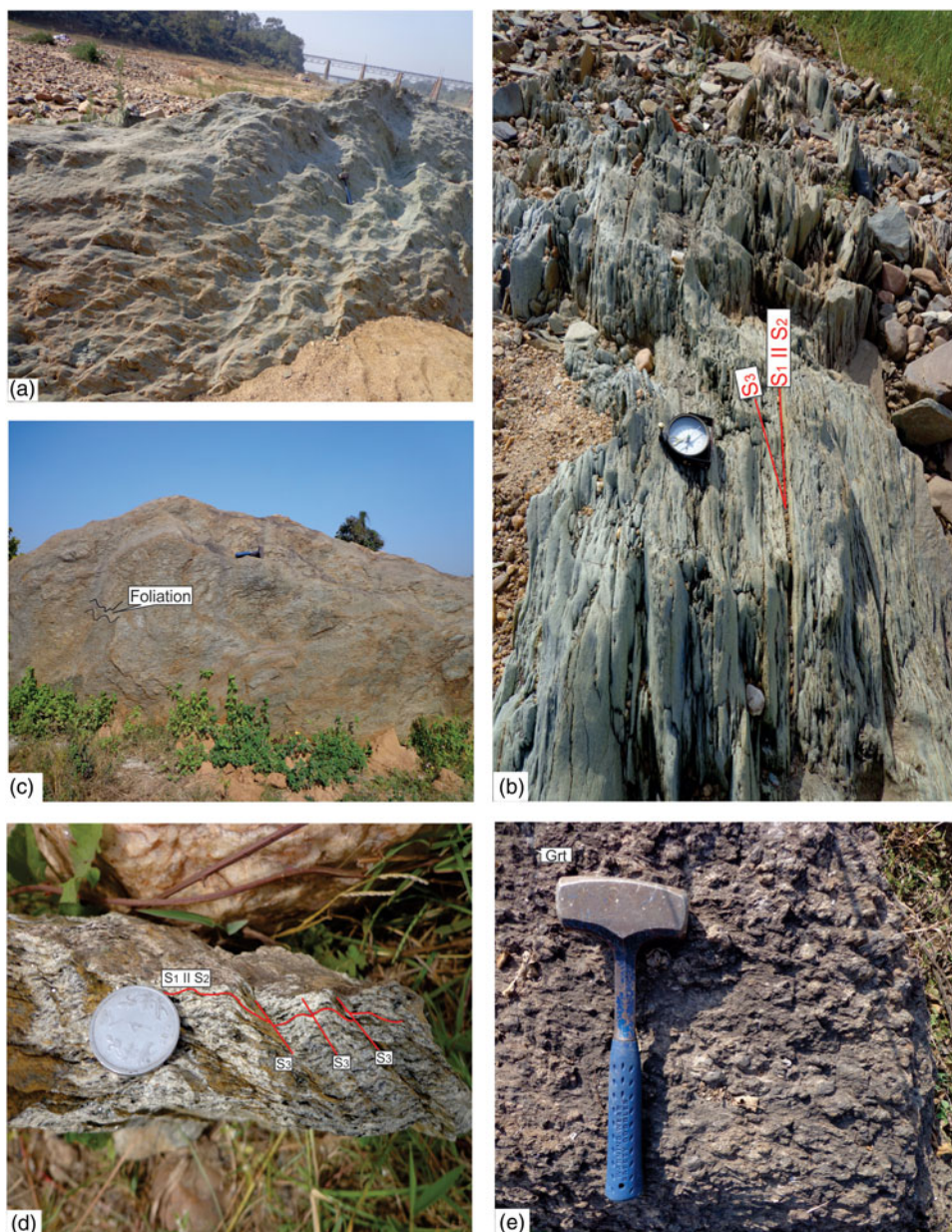


Fig. 2. (Colour online) (a) Field photograph of foliated chlorite phyllite at Subarnarekha river. (b) Chlorite phyllite showing light green colour with S_1 bedding plane parallel to the S_2 schistosity plane and S_3 plane makes an acute angle with these planes at Goradih. (c) Feldspathic phyllite near Gidibera. A crude foliation is also present in it. (d) Biotite schist showing intense shearing with S_1 bedding plane parallel to the S_2 schistosity plane and crenulation cleavage S_3 on micro-folded S_2 at Kanki. (e) Garnet-mica schist in which garnet occurs as coarse grains and partly enclosed by the foliation defined by the mica-ceous minerals.



Fig. 3. (Colour online) (a) Highly foliated feldspathic phyllite with folded S_1 and S_2 schistosity showing transposition of planar fabric at hinge zones at Sanjay river in Parbatipur. (b) Silvery feldspathic phyllite at Parbatipur. A crude foliation is also present in it. (c) Outcrop of amphibolite rock at Gopinathpur with three sets of joints J_1 , J_2 and J_3 . (d) Outcrop of folded quartzite with E-W strikes and steep northerly plunging axis near Kandra. (e) Outcrop of garnet-staurolite-mica schist near Bholadih. (f) Outcrop of sillimanite-gneiss with dark-coloured ferromagnesian minerals near Kandra. Garnet occurs as coarse porphyroblast along with fine needle-shaped sillimanite.

geological map. The rare occurrence of kyanite in staurolite indicates that sillimanite is not derived from kyanite and is derived from staurolite (Prakash *et al.* 2017). The metamorphic events in this area show clear evidence of polyphase metamorphism. The main aims of the present paper are (i) to demarcate the study area into different metamorphic zones based on mineral chemistry and discontinuous reactions, (ii) to construct P - T phase equilibria modelling (pseudosections) for the four metamorphic zones delineated, (iii) to propose a P - T gradient followed by the metamorphites of the area, and then (iv) finally the integrated approach will indicate the cause of the regional metamorphism.

2. Geological setting

Existing geochronological data suggest Palaeoproterozoic (~2.2–1.60 Ga) magmatism, metamorphism and deformation with imprints of Mesoproterozoic reactivations registered in different places of northern Singhbhum (Table 1, reviewed in

Chakraborty *et al.* 2015). The supracrustal rocks of Dhanjori, Chaibasa, Dhalbhum, Dalma and Chandil formations are enclosed between the Singhbhum Granitoid (SG) batholith in the south and Chottanagpur Gneissic complex (CGC) in the north and occur as a 200 km long and 50–60 km wide broadly east–west-trending curvilinear belt (Mazumder, 2005; Mazumder *et al.* 2012a, b; Bhattacharya *et al.* 2014). Cooling of the vast volume of Archaean Singhbhum granite possibly induced an isostatic readjustment. The associated tensional regime and deep-seated fractures controlled the formation of the Proterozoic Singhbhum basin. In accordance with Reddy & Evans (2009), the crust was at that time (1900–1800 Ma) thickened and rigid enough to allow surface and internal geological processes comparable to those prevailing today. The Proterozoic volcano-sedimentary succession consists of successively younger Dhanjori, Chaibasa, Dhalbhum, Dalma and Chandil formations of the Singhbhum crustal province record sedimentation and volcanism in a varying tectonic scenario (Mazumder, 2005), hence it assumes immense geological

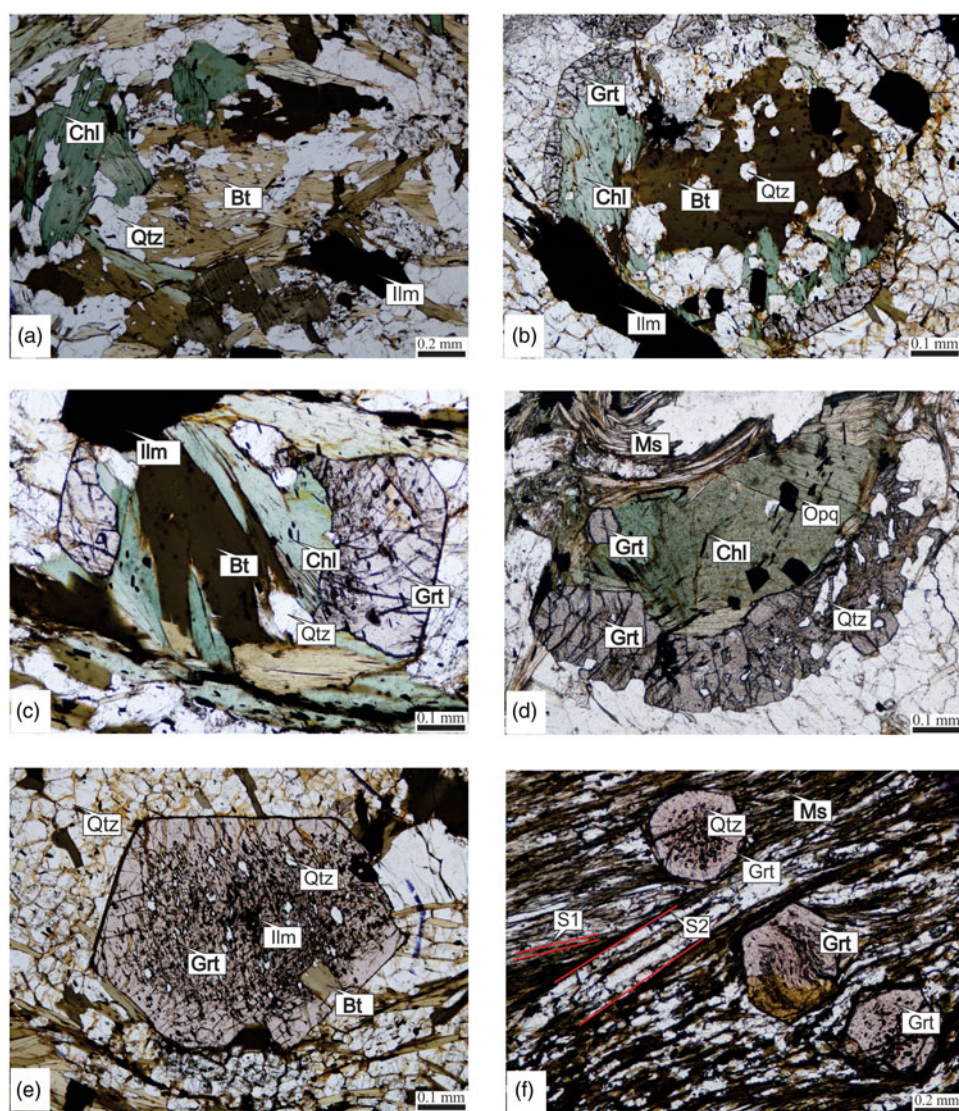


Fig. 4. (Colour online) (a) Well-developed flakes of chlorite and biotite in biotite schist (sample no. S5). (b) The inclusion of biotite and chlorite present at the core of garnet porphyroblast indicating that garnet formed due to the expanse of biotite and chlorite in garnet-biotite-muscovite schist (sample no. SG1). (c) Relict chlorite and biotite within garnet porphyroblast in garnet-biotite-muscovite schist (sample no. SG1). (d) Garnet porphyroblast containing inclusions of biotite, chlorite and ilmenite indicating the formation of garnet from them in garnet-biotite-muscovite schist (sample no. SG1). (e) Post-kinematic poikiloblastic garnet in garnet-biotite-muscovite schist with a late, nearly inclusion-free rim. The core contains the inclusion of ilmenite, muscovite and quartz minerals (sample no. SG1). (f) Dextrally rotated euhehedral garnet porphyroblast and strain slip cleavage produced due to intense shearing. S_1 terminates against S_2 schistosity plane in garnet-biotite-muscovite schist. The texture suggests the growth of the garnet in the centre of the photomicrograph is from pre (the core with inclusions orthogonal to the external foliation) to early (the external free-inclusions rim) to the D_1 tectonic event (sample no. SG1).

significance (Eriksson *et al.* 1999, 2006; Mazumder *et al.* 2000; Mazumder, 2005). According to Sengupta & Chattopadhyay (2004), the Chaibasa Formation is characterized by dominantly arenaceous lithology whereas the Dhalbhum Formation is largely argillaceous. Acharyya *et al.* (2010) suggested the Dhanjori Formation is of Late Archaean – Palaeoproterozoic age (poorly constrained between 2600 and 2100 Ma), and Sarkar *et al.* (1986) assigned the age of the Chaibasa Formation (shallow-marine) as Palaeoproterozoic (*c.* 2200 Ma). Reasonably, shearing along the SSZ is a much younger geological event (*c.* 1600 Ma) than the formation of the units (>2100 Ma) affected by it. The metapelites of the area around Kandra (Fig. 1) belong to the Chaibasa Formation of the Singhbhum Group which represents a part of the Precambrian Orogenic cycle of Singhbhum region (Dunn & Dey, 1942; Naha, 1961; Mazumder *et al.* 2012a, b; Chakraborty *et al.* 2015). Structurally, the area represents the southern portion of the Singhbhum anticlinorium of the Singhbhum fold belt and is separated from the low-grade metamorphic rocks of the southern Singhbhum by a major shear zone designated as the Singhbhum Shear Zone (SSZ) (Fig. 1a). The region north of the SSZ is characterized by a sequence of mica schist, often garnetiferous, with numerous bands of amphibolite, hornblende schist and quartzite,

metamorphosed to amphibolite facies. Dunn & Dey (1942) grouped these formations into the ‘Chaibasa’ stage and placed them in the lower part of the Iron Ore Series. Iyengar & Murthy (1982) renamed this stage as Ghatsila Formation, and Sarkar & Saha (1962) placed them in the Singhbhum Group. Huge basic magmatism took place during the extensional event which is represented by the Dhanjori and Dalma formations and may be represented as the first stage of the Palaeoproterozoic volcanics (Fig. 1a). In the northern part, these sequences are overlain by a sequence of low-grade rocks comprising magnetite phyllite, chlorite schist, carbon phyllite and orthoquartzite forming a belt south of the Dalma Volcanics. They have been called the Dhalbhum Formation (Table 1) and placed in the Singhbhum Group by Sarkar & Saha (1962). Finally, the volcano-sedimentary protolith of the North Singhbhum Fold belt was deformed and metamorphosed during the second phase of orogenesis (Fig. 1a).

In the study area, three types of planar structures have been recognized: (i) the bedding S_1 , (ii) the axial plane foliation S_2 on bedding S_1 (Fig. 2b) and (iii) crenulation cleavage S_3 on microfolded S_2 (Fig. 2d). The area displays two phases of deformation (D_1 and D_2) and two episodes of the medium-pressure type of metamorphism (M_1 and M_2). During the first phase of deformation (D_1), the rocks

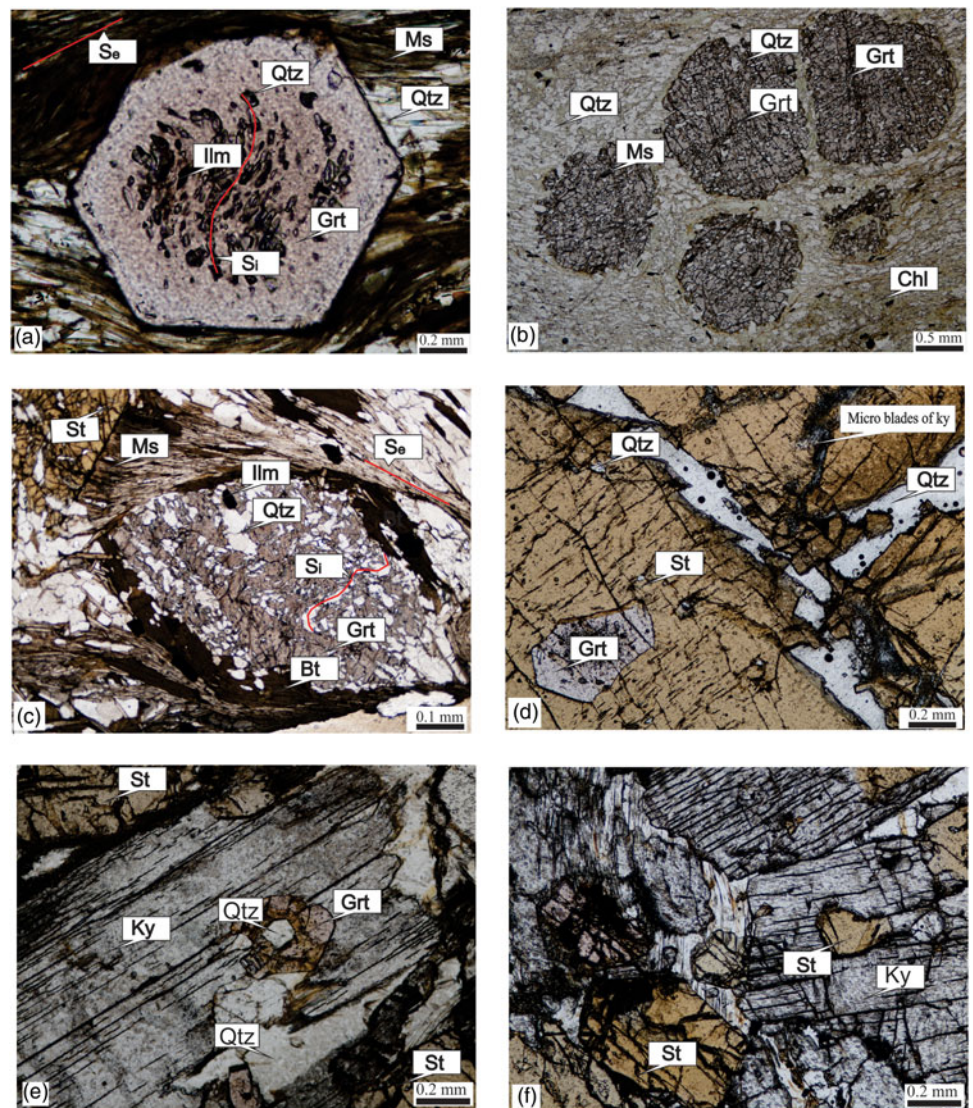


Fig. 5. (Colour online) (a) Photomicrograph of garnet–biotite–muscovite schist (sample no. SG1) showing inclusion-rich core with Si discordant with S_e , surrounded by the inclusion-free rim in dextrally rotated garnet porphyroblast (sample no. SG1). (b) Fractured and rounded garnet porphyroblasts with inclusions of quartz and opaque in chloritic groundmass in garnet–muscovite–chlorite schist (sample no. SG1). (c) Oval-shaped highly poikiloblastic garnet containing linear Si of inequant quartz discordant with the foliation S_e encloses the poikiloblastic garnet. The texture suggests the growth of the garnet in the centre of the photomicrograph is from pre (the core with inclusions orthogonal to the external foliation) to early (the external free-inclusions rim) to the D_1 tectonic event (sample no. K14). (d) Large porphyroblasts of staurolite with inclusions of garnet and microblades of kyanite in garnet–staurolite–mica schist (sample no. K14). (e) Large blades of kyanite with the inclusion of garnet in garnet–staurolite–mica schist (sample no. K14). (f) Blades of kyanite with the inclusion of staurolite and in contact with staurolite in garnet–staurolite–mica schist (sample no. K14).

were folded in E–W-trending isoclinal folds (F_1) overturned to the south, and the foliation S_2 developed. D_1 is superimposed by D_2 which folded the limbs of F_1 folds and formed northerly-trending folds (F_2) and the crenulation cleavage S_3 . The restricted study area falls within the domain sharing all the above-mentioned features; however, the rocks exposed in the study area incorporating fine- to medium-grained schistose rock display only a few partially developed features which can be clearly seen at the regional scale (Mahadevan, 2002). The M_1 phase of metamorphism falls prior to the D_1 phase of deformation and S_2 tectonic fabric development, whereas the M_2 metamorphic episode is associated with a late to post- D_2 deformation event and is synchronous with S_2 fabric evolution (Mahato *et al.* 2008).

The dominant rock types are metapelites (chlorite–biotite schist/phyllite, garnet/chlorite mica schist, staurolite–garnet–kyanite schist, sillimanite–garnet–mica schist) with occasional intercalations of metabasics (amphibolite). In this area, joints are well developed in amphibolites and quartzites (Fig. 3c). A few discontinuous micaceous quartzite bands (Fig. 3d) and lenses of quartz and kyanite within the metapelites have also been found. These rocks are metamorphosed by a regional event of metamorphism and show the highest grade in the south-central and central

portion of the area, gradually decreasing towards the NNE and SSW. Key-horizon layers and top-to-bottom sedimentary structures are absent, making it difficult to establish the detailed stratigraphy of the study area. However, broad parallelism exists between the isograds and the axial trends of the regional folds. Spatial variation in metamorphic conditions of this area has been shown in the zonal map Figure 1b, whereupon the attitudes of different structural elements are superimposed. The isograds have been drawn chiefly on the basis of the first appearance of the index minerals. Kyanite in the present area has sporadic occurrence and does not follow any pattern.

3. Sample description

A detailed field study has revealed the presence of different rocks in different zones which are grouped as follows:

- i Biotite zone – Biotite schist (S_5)
- ii Garnet zone – Garnet–biotite–muscovite schist (SG1)
- iii Staurolite zone – Garnet–staurolite–chlorite–mica schist (K13)
- iv Staurolite zone – Staurolite–mica schist (K14)
- v Sillimanite zone – Sillimanite schist (SS1)

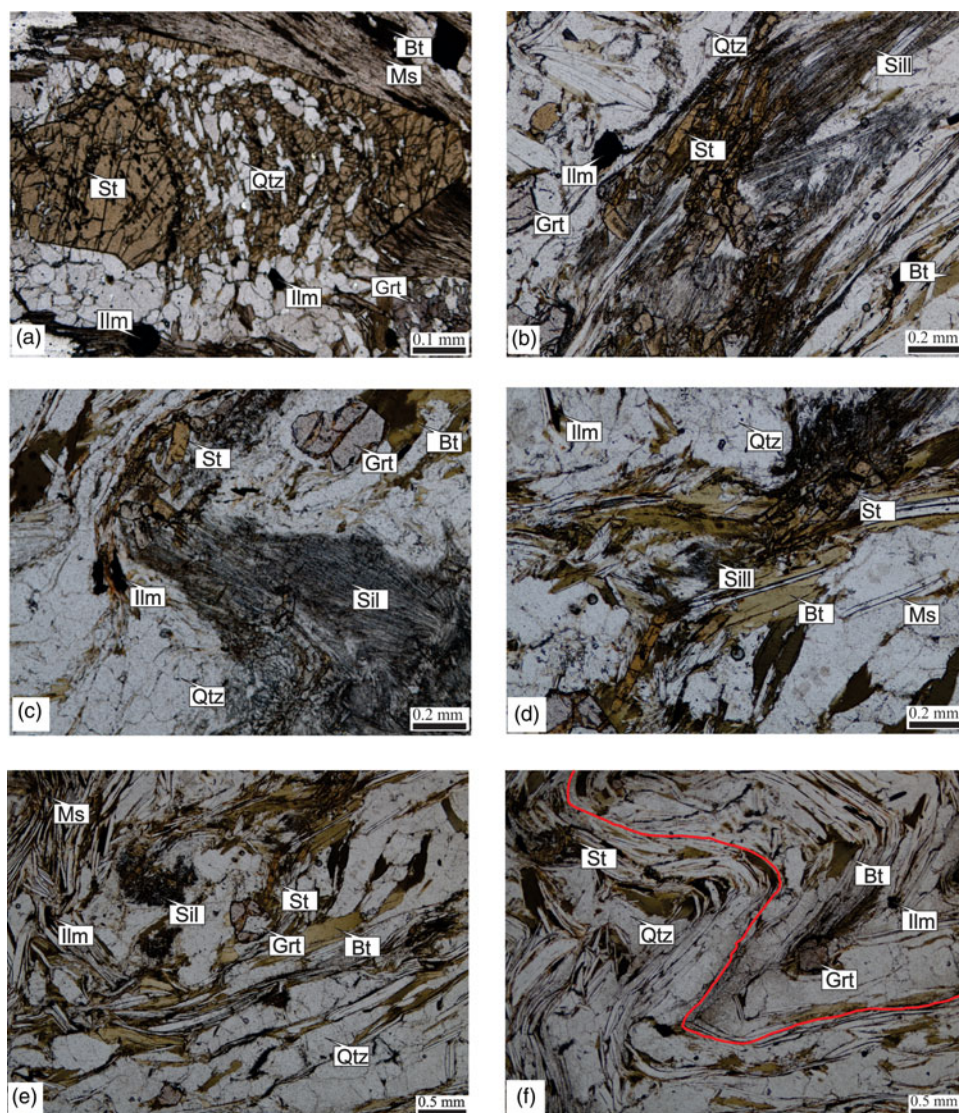


Fig. 6. (Colour online) (a) Sieved staurolite containing linear Si of inequant quartz discordant with the foliation S_2 encloses the poikiloblastic staurolite in garnet-biotite-muscovite schist (sample no. K14). (b) Relict garnet porphyroblast replaced by fibrolite occurs along with biotite in sillimanite schist (sample no. SS1). (c) Fibrolite with relics of staurolite and post-tectonic garnet in sillimanite schist (sample no. SS1). (d) Relict staurolite replaced by fibrolite occurs along with biotite and muscovite foliation in sillimanite schist (sample no. SS1). (e) Sillimanite intergrowth along with muscovite, staurolite, garnet, in sillimanite schist (sample no. SS1). (f) Microfolding of the foliation S_2 with relics of staurolite and post-tectonic garnet in sillimanite schist (sample no. SS1).

3.a. Biotite zone

The rocks of this zone include schists, phyllites, and quartzite with or without kyanite. Phyllites and biotite schist are well exposed around Subarnrekha river c. 8 km NE of Kandra town. Phyllites are foliated metamorphic, shiny, fine-grained rocks consisting of white mica which shows preferred orientation. Primarily it is composed of quartz, chlorite and sericite mica. It belongs to low-grade metamorphic rock and shows a gradation in the degree of metamorphism between slate and schist. Biotite schist is schistose in character with a dazzling silvery-white or golden-green surface (Fig. 2a, b). The chlorite mica schist is green in colour and is punctuated by the occurrence of quartz veins and lenses (Fig. 2c). Foliation (S_2) is defined by the parallel orientation of white mica and chlorite. In few specimens, mineral lineation is observed on the S_3 foliation defined by elongation of chlorite flakes. With an increase in the amount of feldspar, the phyllites grade into feldspathic phyllite (Fig. 3b) in which augens of feldspar are conspicuous. Sometimes, chlorite occurs as discontinuous patches and streaks within the quartzo-feldspathic mass. The phyllites grade into mica schist in the vicinity of the garnet isograd, and the biotite schist consists of biotite, chlorite, muscovite and quartz (Fig. 2d).

3.b. Garnet zone

Garnet-biotite-muscovite schist is exposed c. 5 km north of Raipur and Gidibera. It also occurs c. 20 km south of Kandra in and around Gangpur. The garnet-biotite-muscovite schists of this zone are medium- to coarse-grained, light green to greenish grey in colour due to the predominance of chlorite. Garnet, chlorite, muscovite and quartz are the predominant constituent minerals in the rock. Garnet ranges in size from 0.5 mm to c. 2.0 mm (Fig. 2e). Garnet-biotite-muscovite schists are medium- to fine-grained rock with distinct schistosity defined by the arrangement of biotite and muscovite flakes (Fig. 3a).

3.c. Staurolite zone

The staurolite zone marked by garnet-staurolite-chlorite-mica schist extends from 18 km south around Sobhapur and also in and around Kandra town. It is also exposed near Ramchandrapur which is c. 5 km SE of Kandra. The lithotype recording the staurolite zone is staurolite-garnet-mica/kyanite schists. The schists of this zone are coarse-grained, brown-coloured rock with well-developed S_2 schistosity marked by oriented muscovite and biotite (Fig. 3e). Large staurolite

Table 2. Representative analyses of garnet (12 oxygen basis)

Rock types	Grt–Bt–Ms schist				Grt–St–Chl–mica schist		Grt–St–mica schist		Sil schist	
Metamorphic zones	Garnet zone				Staurolite zone		Staurolite zone		Sillimanite zone	
Sample no.	SG1	SG1	SG1	SG1	K13	K13	K14	K14	SS1	SS1
Domain	C	R	C	R	C	R	C	R	C	R
SiO ₂	36.28	36.31	36.74	37.45	38.01	37.24	37.53	36.81	36.81	36.11
TiO ₂	0.27	0.19	0.31	0.19	0.13	0.07	0.22	0.19	0.31	0.21
Al ₂ O ₃	18.57	19.13	18.81	18.87	19.07	17.55	18.15	16.81	19.24	18.34
FeO	35.71	34.81	34.84	35.64	35.61	37.75	35.20	38.35	35.57	34.34
MnO	3.85	3.14	3.81	1.46	1.71	1.31	1.51	1.61	3.13	3.87
MgO	2.31	2.87	2.91	3.02	3.11	3.27	3.19	3.61	3.51	3.81
CaO	2.84	2.72	2.23	3.13	2.81	2.51	2.58	2.04	1.11	2.97
Total	99.83	99.17	99.65	99.76	100.45	99.70	98.38	99.42	99.68	99.65
Si	2.99	2.99	3.01	3.05	3.07	3.06	3.09	3.05	3.01	2.97
Ti	0.02	0.01	0.02	0.01	0.01	0.00	0.01	0.01	0.02	0.01
Al	1.81	1.86	1.82	1.81	1.81	1.70	1.76	1.64	1.85	1.78
Fe	2.46	2.40	2.39	2.43	2.40	2.60	2.42	2.66	2.43	2.36
Mn	0.27	0.22	0.26	0.10	0.12	0.09	0.11	0.11	0.22	0.27
Mg	0.28	0.35	0.36	0.37	0.37	0.40	0.39	0.45	0.43	0.47
Ca	0.25	0.24	0.20	0.27	0.24	0.22	0.23	0.18	0.10	0.26
X _{Mg}	0.11	0.13	0.14	0.14	0.14	0.14	0.15	0.16	0.16	0.18

X_{Mg} = Mg/(Mg + Fe²⁺); C - core; R - rim;

Grt = garnet, Bt = biotite, Ms = muscovite, Chl = chlorite, St = staurolite, Sil = sillimanite.

crystals, ranging in size from 0.5 to 2.5 mm length, are fairly abundant. They show random orientation along the S₂ foliation. Garnet crystals range in size from 0.5 to 2.0 mm in diameter and are fairly abundant.

3.d. Sillimanite zone

Sillimanite schist is well exposed around Raghunathpur and Karangura, 2 km north of Kandra. It is also observed at Bhaduagora, Pathargora and Nandidih to the south of Kandra town. The sillimanite-bearing schists are light to dark grey in colour and are coarse-grained with well-developed S₂ foliation defined by the parallel alignment of micas interlayered with quartzite (Fig. 3d). Sillimanite is fine-needle-shaped (Fig. 3f) and staurolite crystals are smaller in grain size. Garnet crystals range in size from 0.5 mm to c. 2 mm in diameter.

4. Textural relationship

4.a. Biotite zone

The rocks of this zone include schists, phyllites, and quartzite with or without kyanite. Prograde chlorite (0.10 to 1.4 mm long) occurs in the biotite zone. Coarse flakes of chlorite are interlayered with muscovite and biotite along S₂ foliation (Fig. 4a). The quartzites are of grey, light brown or yellow colour, medium-grained and consist predominantly of quartz, sericite and chlorite.

4.b. Garnet zone

In thin-section, S₁ foliation is deformed by tight F₂ micro-folding associated with an S₂ axial-plane schistosity. Resorbed chlorite and biotite are present at the core of the garnet porphyroblast, indicating prograde crystallization of garnet from chlorite and biotite (Fig. 4b, c, d). In thin-sections, micas define the main foliation (S₂) and wrap the garnet crystal, so garnet growth pre-dates the foliation. The core of the garnet with sigmoidal inclusions (but not continuing in the external foliation) points to a pre-D₁ tectonic event (Fig. 4f). Garnet grains commonly occur as porphyroblasts, which are xenoblastic and sieved with inclusions of quartz, biotite, muscovite and ilmenite (Fig. 4e). At times, small idioblastic to sub-idioblastic grains, with their rim free of any inclusion, are also present (Fig. 4f). Garnet is characterized by spiral or rotational S₁ defined by inequant quartz and ilmenite. The foliation S₂ wraps around garnet with pressure shadow areas of quartz (Fig. 5a).

Near the staurolite–biotite isograd, the size of the garnet increases significantly (up to 1.0 mm in diameter). Besides the prograde crystallization of chlorite, its retrograde formation from garnet and biotite is also seen, where the garnet xenoblasts are enclosed within chlorite mass (Fig. 5b).

4.c. Staurolite zone

The lithotype recording the staurolite zone is staurolite–garnet–mica/kyanite schists. In a thin-section, the S₂ foliation shows prominent microfolding associated with the development of an S₃ axial plane foliation that can be classified as crenulation

Table 3. Representative analyses of chlorite (28 oxygen basis)

Rock types	Biotite schist		Grt–Bt–Ms schist		Grt–St–Chl–mica schist		Gt–St–mica schist		
Metamorphic zones	Biotite zone		Garnet zone		Staurolite zone		Staurolite zone		
Sample no.	S5	S5	SG1	SG1	K13	K13	K14	K14	K14
Domain	C	R	C	R	C	R	C	C	R
SiO ₂	26.05	26.17	24.46	24.47	23.63	23.99	24.39	23.87	23.79
TiO ₂	0.06	0.02	0.00	0.19	0.00	0.02	0.09	0.09	0.00
Al ₂ O ₃	21.29	21.15	22.49	22.87	22.61	23.80	22.87	23.37	22.21
FeO	21.67	21.93	22.23	24.55	24.11	25.18	24.86	23.47	23.84
MnO	0.16	0.22	0.10	0.20	0.24	0.16	0.08	0.19	0.19
MgO	16.83	15.83	15.70	14.52	14.01	14.10	14.73	13.93	13.98
CaO	0.06	0.10	0.06	0.06	0.04	0.05	0.09	0.06	0.19
Na ₂ O	0.03	0.01	0.02	0.00	0.00	0.00	0.03	0.08	0.05
K ₂ O	0.00	0.02	0.01	0.00	0.00	0.00	0.01	0.00	0.13
Cr ₂ O ₃	0.00	0.00	0.06	0.00	0.00	0.00	0.00	0.00	0.00
Total	86.15	85.44	85.09	86.86	84.64	87.29	87.14	85.06	84.38
Si	5.46	5.53	5.22	5.18	5.14	5.07	5.16	5.13	5.19
Ti	0.01	0.00	0.00	0.03	0.00	0.00	0.01	0.01	0.00
Al ^{IV}	2.54	2.47	2.78	2.82	2.86	2.93	2.84	2.87	2.81
Al ^{VI}	2.73	2.82	2.89	2.90	2.95	3.01	2.86	3.07	2.91
Fe ³⁺	0.11	0.19	0.06	0.07	0.05	0.05	0.02	0.11	0.03
Fe ²⁺	3.69	3.68	3.91	4.27	4.34	4.41	4.38	4.11	4.32
Mn	0.03	0.04	0.02	0.04	0.04	0.03	0.01	0.04	0.04
Mg	5.26	4.99	5.00	4.58	4.55	4.44	4.65	4.47	4.54
Ca	0.01	0.02	0.01	0.01	0.01	0.01	0.02	0.01	0.04
Na	0.03	0.01	0.02	0.00	0.00	0.00	0.03	0.07	0.04
K	0.00	0.01	0.01	0.00	0.00	0.00	0.00	0.00	0.07
Cr	0.00	0.00	0.01	0.00	0.00	0.00	0.00	0.00	0.01
X _{Mg}	0.58	0.56	0.56	0.51	0.51	0.50	0.51	0.51	0.51

X_{Mg} = Mg/(Mg + Fe²⁺); C – core; R – rim;

Grt = garnet, Bt = biotite, Ms = muscovite, Chl = chlorite, St = staurolite, Sil = sillimanite.

cleavage. Skeletal xenoblastic crystals of highly sieved garnet, with coarse equant inclusions of quartz which are comparable in grain size to the quartz occurring in the matrix, are very common in this zone (Fig. 5c). The textural relations suggest that growth of garnet occurred after the development of S₁ foliation, with respect to D₁ deformation. The inclusion of garnet occurs in staurolite (Fig. 5d), which suggests the crystallization of garnet preceded that of staurolite. Locally, garnet and staurolite occur as inclusions within kyanite, indicating prograde metamorphism (Fig. 5e, f). Staurolite also occurs as xenoblasts enclosed within an aggregate of biotite and muscovite or in coarse porphyroblasts of muscovite (Fig. 6a).

4.d. Sillimanite zone

These rocks show schistose lepidoblastic texture with well-developed S₂ schistosity, which is defined by the parallel orientation of muscovite and biotite. Sometimes, S₂ is micro-folded with the

development of S₃ crenulation cleavage at high angles. Biotite and muscovite flakes are sharply folded along these microfolds, and ilmenite follows the orientation of mica along these microfolds. Few muscovite flakes are found oriented parallel to the axial plane of the S₂ fold. Sillimanite commonly occurs as fibrolite mats (Fig. 6b, c). In one sample, i.e. sillimanite–garnet–biotite schist that is devoid of muscovite, coarse radiating needles of sillimanite have been observed. Fibrolites are randomly oriented and intimately intergrown with biotite or muscovite or both (Fig. 6d). Fibrolite also occurs at the grain borders of garnet, quartz and as inclusions within it. Fibrolite mats are deformed and folded along with the microfolded S₂ foliation (Fig. 6e, f). The textural features described above indicate post-tectonic crystallization of fibrolite and sillimanite with respect to D₁. Mostly, sillimanite occurs as fibrolite mats intergrown with staurolite in this zone. Textural features indicate the formation of sillimanite from the breakdown of staurolite (Fig. 6e).

Table 4. Representative analyses of biotite (22 oxygen basis)

Rock types	Biotite schist		Grt–Bt–Ms schist		Grt–St–Chl–mica schist		Gt–St–mica schist		Sil schist	
Metamorphic zones	Biotite zone		Garnet zone		Staurolite zone		Staurolite zone		Sillimanite zone	
Sample no.	S5	S5	SG1	SG1	K13	K13	K14	k14	SS1	SS1
Domain	C	R	C	R	C	R	C	R	C	R
SiO ₂	35.06	35.30	35.55	35.61	37.14	35.78	35.45	34.84	34.91	37.49
TiO ₂	1.60	1.64	2.10	1.43	1.73	1.68	1.54	1.30	1.90	1.91
Al ₂ O ₃	17.38	17.90	18.76	17.37	17.59	18.36	18.62	19.03	18.31	20.83
Cr ₂ O ₃	0.08	0.08	0.18	0.05	0.19	0.13	0.14	0.12	0.21	0.18
FeO	22.55	20.77	19.78	21.23	20.14	18.61	18.29	19.31	18.71	15.12
MnO	0.23	0.05	0.33	0.01	0.21	0.13	0.16	0.11	0.27	0.14
MgO	9.61	9.05	8.79	9.24	10.43	10.38	10.23	12.05	13.07	11.44
CaO	0.09	0.14	0.28	0.06	0.23	0.09	0.17	0.87	0.95	0.32
Na ₂ O	0.13	0.28	0.42	0.31	0.36	0.35	0.38	1.44	1.51	0.56
K ₂ O	7.63	8.40	7.81	8.44	8.10	8.30	8.48	8.01	7.92	7.82
Total	94.36	93.61	94.01	93.75	96.13	93.81	93.47	97.08	97.76	95.80
Si	5.40	5.44	5.41	5.49	5.49	5.43	5.41	5.18	5.15	5.39
Ti	0.19	0.19	0.24	0.17	0.19	0.19	0.18	0.15	0.21	0.21
Al ^{IV}	2.60	2.56	2.59	2.51	2.51	2.57	2.59	2.82	2.85	2.61
Al ^{VI}	0.55	0.70	0.77	0.64	0.56	0.71	0.76	0.52	0.33	0.92
Cr	0.01	0.01	0.02	0.01	0.02	0.02	0.02	0.01	0.02	0.02
Fe	2.90	2.68	2.52	2.74	2.49	2.36	2.33	2.40	2.31	1.82
Mn	0.03	0.01	0.04	0.00	0.03	0.02	0.02	0.01	0.03	0.02
Mg	2.21	2.08	1.99	2.12	2.30	2.35	2.33	2.67	2.87	2.45
Ca	0.02	0.02	0.05	0.01	0.04	0.01	0.03	0.14	0.15	0.05
Na	0.04	0.08	0.12	0.09	0.10	0.10	0.11	0.42	0.43	0.16
K	1.50	1.65	1.52	1.66	1.53	1.61	1.65	1.52	1.49	1.43
X _{Mg}	0.43	0.44	0.44	0.44	0.48	0.50	0.50	0.53	0.55	0.57

X_{Mg} = Mg/(Mg + Fe²⁺); C – core; R – rim;

Grt = garnet, Bt = biotite, Ms = muscovite, Chl = chlorite, St = staurolite, Sil = sillimanite.

5. Mineral chemistry

The mineral chemistry was carried out by a CAMECA-SX Five electron microprobe (EPMA) at the Department of Geology, Banaras Hindu University, Varanasi. Wavelength-dispersive spectrometry and a LaB6 filament have been deployed for quantitative analyses. An accelerating voltage of 15 kV, a beam current of 10 nA and a beam diameter of 1 µm along with TAP, LPET and LLIF crystals were employed for measurement. A number of natural and synthetic standards were used for calibration. After repeated analyses, it was found that the error on major element concentrations is less than 1 % of each oxide's weight per cent. Representative mineral chemistry of various phases is provided in Tables 2–8.

5.a. Garnet

Garnet consists mainly of almandine component which ranges from 68 to 77 %. In these garnets, pyrope, spessartine and grossularite components range from 10 to 15 %, 3 to 9 % and 1 to 5 %

respectively. In the area around Kandra, bulk EPMA analysis of the garnet indicates an increase in MnO% of garnet from the staurolite towards the high-grade sillimanite zone and also towards the low-grade garnet zone. The [Mg/(Mg + Fe²⁺) = X_{Mg}] varies from 0.11 to 0.14 in the garnet zone, 0.14 to 0.16 in the staurolite zone and 0.16 to 0.18 in the sillimanite zone. It is evident that there is a gradual increase of X_{Mg} in the garnet with increasing grade of metamorphism. Based on stoichiometric considerations, the andradite component was found to be <5 %.

5.b. Chlorite

As the chlorites of the area are analysed by microprobe, the content of Fe³⁺ is calculated stoichiometrically. However, the ubiquitous presence of magnetite possibly suggests moderate Fe³⁺ in these chlorites (up to 0.2 per formula unit (pfu)). Thus, it is assumed that the chlorites belong to the oxidized class. The plots of the analyses of the chlorite show that these are mainly ripidolite.

Table 5. Representative analyses of muscovite (22 oxygen basis)

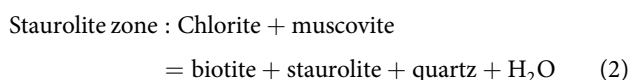
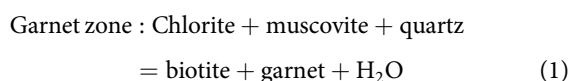
Rock types	Biotite schist		Grt-Bt-Ms schist		Grt-St-Chl-mica schist		Gt-St-mica schist		Sil schist	
Metamorphic zoneS	Biotite zone		Garnet zone		Staurolite zone		Staurolite zone		Sillimanite zone	
Sample no.	S5	S5	SG1	SG1	K13	K13	K14	K14	SS1	SS1
Domain	C	R	C	R	C	R	C	R	C	R
SiO ₂	46.60	45.26	46.93	46.36	45.54	47.28	46.83	48.25	47.92	47.54
TiO ₂	0.13	0.03	0.22	0.31	0.18	0.27	0.36	0.36	0.24	0.35
Al ₂ O ₃	36.26	33.79	35.41	34.05	35.75	36.09	34.66	33.85	34.85	34.42
Cr ₂ O ₃	0.03	0.00	0.03	0.10	0.02	0.05	0.11	0.06	0.00	0.08
FeO	2.22	2.42	1.87	2.30	2.07	1.90	2.08	1.92	1.54	2.14
MnO	0.08	0.00	0.00	0.13	0.06	0.06	0.03	0.03	0.00	0.06
MgO	0.51	0.57	0.50	0.60	0.58	0.53	0.60	0.59	0.64	0.77
CaO	0.06	0.14	0.10	0.06	0.20	0.17	0.15	0.14	0.03	0.08
Na ₂ O	1.18	1.40	1.20	0.96	1.29	1.18	1.25	0.80	1.23	1.09
K ₂ O	6.69	8.50	8.18	7.89	7.82	6.18	7.39	7.77	7.93	6.99
Total	93.76	92.12	94.45	92.76	93.51	93.70	93.47	93.78	94.38	93.51
Si	6.19	6.22	6.23	6.28	6.12	6.25	6.27	6.42	6.34	6.33
Ti	0.01	0.00	0.02	0.03	0.02	0.03	0.04	0.04	0.02	0.03
Al ^{IV}	1.81	1.78	1.77	1.72	1.88	1.75	1.73	1.58	1.66	1.67
Al ^{VI}	3.86	3.69	3.78	3.71	3.78	3.87	3.74	3.73	3.77	3.74
Cr	0.00	0.00	0.00	0.01	0.00	0.01	0.01	0.01	0.00	0.01
Fe	0.25	0.28	0.21	0.26	0.23	0.21	0.23	0.21	0.17	0.24
Mn	0.01	0.00	0.00	0.01	0.01	0.01	0.00	0.00	0.00	0.01
Mg	0.10	0.12	0.10	0.12	0.12	0.11	0.12	0.12	0.13	0.15
Ca	0.01	0.02	0.01	0.01	0.03	0.02	0.02	0.02	0.00	0.01
Na	0.30	0.37	0.31	0.25	0.34	0.30	0.32	0.21	0.32	0.28
K	1.13	1.49	1.39	1.36	1.34	1.04	1.26	1.32	1.34	1.19
X _{Mg}	0.29	0.30	0.32	0.32	0.33	0.33	0.34	0.35	0.43	0.39

X_{Mg} = Mg/(Mg+Fe²⁺); C - core; R - rim;

Grt = garnet, Bt = biotite, Ms = muscovite, Chl = chlorite, St = staurolite, Sil = sillimanite.

The aluminium contents of chlorite from different zones range between 21 and 24 wt % and do not reveal any significant change with the grade of metamorphism. The high Al content of the chlorites from the Kandra area is related to the ubiquitous association of these chlorites with muscovite and sericite.

The X_{Mg} values in the chlorites vary from 0.51 to 0.58 in the biotite/garnet zone and 0.50 to 0.51 in the staurolite zone. Chlorite is expected in rocks of similar bulk composition through continuous reaction:



This feature is evident when the chlorites of the biotite/garnet zone and the staurolite zone are compared. Considerably higher

X_{Mg} in the chlorite in the biotite/garnet zone compared to that in the staurolite zone suggests the effect of bulk composition in controlling this ratio because the textural features suggest crystallization of chlorite during the syntectonic phase of D₁ deformation, while in the higher-temperature zones it reacted with other minerals and disappeared. This feature can also be controlled by oxygen fugacity (Zane *et al.* 1998), as well as composition of altered minerals, such as amphibole, biotite, etc., but bulk composition as controlling factor seems to be more appropriate in the present case.

5.c. Biotite

The X_{Mg} in the biotite varies in the different zones as follows: 0.43 to 0.44 in the biotite zone, 0.44 in the garnet zone, 0.48 to 0.53 in the staurolite zone, 0.55 to 0.57 in the sillimanite zone, showing a slight increase in the X_{Mg} of biotite with the grade of metamorphism in the area. The Ti content is almost constant

Table 6. Representative analyses of staurolite (23 oxygen basis)

Rock types	Gt–St–mica schist					Sil schist	
Metamorphic zones	Gt–St–Chl mica schist		Staurolite zone			Sillimanite zone	
Sample no.	K13	K13	K14	K14	K14	SS1	SS1
Domain	R	C	C	R	R	C	R
SiO ₂	27.28	26.64	26.78	29.53	24.15	27.48	26.88
TiO ₂	0.34	0.36	0.30	0.34	0.55	0.46	0.35
Al ₂ O ₃	54.14	53.60	53.31	53.14	55.89	52.61	54.19
Cr ₂ O ₃	0.00	0.00	0.00	0.01	0.06	0.00	0.04
FeO	14.33	14.42	14.25	13.69	14.10	14.22	13.62
MnO	0.11	0.04	0.22	0.31	0.29	0.15	0.35
MgO	1.76	1.79	1.75	1.79	1.60	1.81	1.77
CaO	0.00	0.00	0.02	0.03	0.14	0.00	0.05
Na ₂ O	0.05	0.02	0.02	0.02	0.02	0.03	0.02
Total	98.02	96.88	96.66	98.87	96.80	96.75	97.26
Si	4.04	3.79	3.75	3.76	3.87	3.78	3.42
Ti	0.03	0.04	0.04	0.04	0.05	0.03	0.06
Al	8.58	8.87	8.90	8.93	8.74	8.86	9.32
Cr	0.00	0.00	0.00	0.00	0.00	0.00	0.01
Fe ²⁺	1.57	1.67	1.70	1.59	1.68	1.68	1.67
Mn	0.04	0.01	0.00	0.04	0.02	0.03	0.03
Mg	0.37	0.37	0.38	0.37	0.38	0.37	0.34
Ca	0.00	0.00	0.00	0.01	0.00	0.00	0.02
Na	0.01	0.01	0.01	0.01	0.01	0.01	0.01
X _{Mg}	0.19	0.18	0.18	0.19	0.18	0.18	0.17

X_{Mg} = Mg/(Mg + Fe²⁺); C – core; R – rim;

Grt = garnet, Bt = biotite, Ms = muscovite, Chl = chlorite, St = staurolite, Sil = sillimanite.

from the biotite zone to the staurolite zone but it is considerably higher in the sillimanite zone.

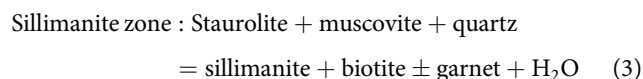
5.d. Muscovite

Chemical analysis shows that there is a gradual increase of X_{Mg} in muscovite with increasing grade of metamorphism. The muscovites of the Kandra area contain 0.03–0.36 TiO₂ pfu and do not show any correlation with grade of metamorphism. There is a general decrease in the TiO₂ content of muscovite with the modal rise in muscovite–biotite/chlorite + staurolite. Thus, the TiO₂ content of these muscovites shows a correlation with the host rock composition. Guidotti (1970) has shown that the jump in Ti content of muscovite coincides with a sharp modal decrease in muscovite, on the basis of which he suggested that the increase in Ti content of micas is primarily due to the concentration effect which results in a modal decrease in muscovite and hence total mica. The phengitic content is recognized by higher trisilic muscovite (i.e. more than 6.00 pfu on the basis of 22 oxygens). Reaction (1), although it explains the association of garnet–muscovite–chlorite–biotite in pelitic rocks of the garnet zone in the Kandra area, does not take into consideration the reduction in the phengitic component of white mica which is evident from the comparison of the biotite and garnet zones of

the Kandra area. It is therefore proposed that reaction (1) explains the observed mineralogical assemblage in the garnet zone pelites of the area.

5.e. Staurolite

The X_{Mg} values in the staurolite range from 0.18 to 0.19 in the staurolite zone and 0.18 to 0.17 in the sillimanite zone. Thus, X_{Mg} decreases from the staurolite to the sillimanite zone. Similarly, the decrease in X_{Mg} of the staurolite from staurolite zone to sillimanite zone (and also from the core to the rim) may be attributed to continuous reaction:



5.f. Feldspar

The X_{An} content of plagioclase feldspar has been determined by microprobe and varies in different zones as follows: biotite zone 0.22, garnet zone 0.24, staurolite zone 0.25–0.27 and sillimanite 0.29. The X_{Or} content of K-feldspar ranges from 0.60 to 0.73 in sillimanite schist.

Table 7. Representative analyses of plagioclase (8 oxygen basis)

Rock types	Biotite schist		Gt-Bt-Ms schist		Grt-St-Chl-mica schist		Grt-St-mica schist		Sil schist	
Metamorphic zones	Biotite zone		Garnet zone		Staurolite zone		Staurolite zone		Sillimanite zone	
Sample no.	S5	S5	SG1	SG1	K13	K13	K14	K14	SS1	SS1
Domain	C	R	C	R	C	R	C	R	C	R
SiO ₂	62.62	61.63	61.14	62.93	62.38	61.48	60.22	60.26	62.89	63.32
TiO ₂	0.00	0.00	0.00	0.00	0.00	0.00	0.00	0.00	0.00	0.00
Al ₂ O ₃	23.24	23.58	23.96	23.29	23.89	23.73	25.40	24.34	23.38	23.84
Cr ₂ O ₃	0.00	0.00	0.00	0.00	0.00	0.00	0.00	0.00	0.00	0.00
FeO	0.00	0.00	0.00	0.00	0.00	0.00	0.00	0.00	0.00	0.00
MnO	0.00	0.00	0.00	0.00	0.00	0.00	0.00	0.00	0.00	0.00
MgO	0.00	0.00	0.00	0.00	0.00	0.00	0.00	0.00	0.00	0.00
CaO	4.65	4.55	4.74	4.65	5.29	5.63	5.49	5.46	5.29	5.53
Na ₂ O	9.13	8.74	8.17	8.23	8.56	8.23	9.00	9.05	6.96	7.43
K ₂ O	0.05	0.10	0.09	0.03	0.05	0.05	0.09	0.00	0.04	0.03
Total	99.70	98.50	98.11	99.12	100.18	99.11	100.20	99.12	98.56	100.15
Si	2.78	2.76	2.75	2.80	2.76	2.75	2.68	2.71	2.80	2.78
Ti	0.00	0.00	0.00	0.00	0.00	0.00	0.00	0.00	0.00	0.00
Al	1.22	1.25	1.27	1.22	1.24	1.25	1.33	1.29	1.23	1.24
Cr	0.00	0.00	0.00	0.00	0.00	0.00	0.00	0.00	0.00	0.00
Fe	0.00	0.00	0.00	0.00	0.00	0.00	0.00	0.00	0.00	0.00
Mn	0.00	0.00	0.00	0.00	0.00	0.00	0.00	0.00	0.00	0.00
Mg	0.00	0.00	0.00	0.00	0.00	0.00	0.00	0.00	0.00	0.00
Ca	0.22	0.22	0.23	0.22	0.25	0.27	0.26	0.26	0.25	0.26
Na	0.79	0.76	0.71	0.71	0.73	0.71	0.78	0.79	0.60	0.63
K	0.00	0.01	0.01	0.00	0.00	0.00	0.01	0.00	0.00	0.00
An	0.22	0.22	0.24	0.24	0.25	0.27	0.25	0.25	0.29	0.29

$X_{Ca} = Ca/(Ca + Na + K)$; C - core; R - rim;

Grt = garnet, Bt = biotite, Ms = muscovite, Chl = chlorite, St = staurolite, Sil = sillimanite.

6. Metamorphic *P-T* conditions

6.a. Geothermobarometry

An effort has been made to calculate the pressure and temperature (*P-T*) conditions of schists of various zones, viz. biotite zone, garnet zone, staurolite zone and sillimanite zone, of the investigated area simultaneously by using conventional thermobarometry and the winTWQ program. A garnet-biotite thermometer was applied for the garnet zone. The average temperature obtained for the above pair is 525 °C (Fig. 7). The estimated average temperature for a plagioclase - K-feldspar pair for the sillimanite zone is 650 °C (Fig. 7). A simplified thermometer empirically calibrated by Henry *et al.* (2005) based on the Ti content and X_{Mg} in the biotite was applied for different zones. The average temperatures estimated using this thermometer for the biotite, garnet, staurolite and sillimanite zones are 565 °C, 578 °C, 585 °C and 620 °C respectively. Pressure estimates were obtained from a garnet-plagioclase-biotite-muscovite-quartz assemblage employing different calibrations (Fig. 7). The winTWQ program calculates the location of reaction equilibria in *P-T* spaces using the

thermodynamic data of Berman (1988, updated 1991) and Berman & Aranovich (1996) for the end-member phases. Given the offset of end-member phases and a specified *P-T* window, winTWQ calculates all possible equilibria, stable and metastable, applicable to that rock. The end-member phases used in the winTWQ program calculations for the biotite zone include albite, annite, beta-quartz, chlorite, eastonite, hematite, magnetite, muscovite, phlogopite, siderite and water. There are five possible equilibria that can be written for the selected end-member phases. Using these equilibria for sample S5 gives precise intersection (Fig. 8a; Table 9) at 4.4 kbar, 438 °C. The end-member phases used in the winTWQ program calculations for the garnet zone include annite, chlorite, grossular, hematite, K-feldspar, kyanite, magnetite, margarite, muscovite, pyrope and water. There are four possible equilibria that can be written for the selected end-member phases. Using these equilibria, for sample SG1 a precise intersection is obtained (Fig. 8b; Table 9) at 4.9 kbar, 545 °C. The end-member phases used for the staurolite zone include almandine, annite, anorthite, grossular, K-feldspar, phlogopite, pyrope, staurolite and water. Using these equilibria, sample K14 gives precise intersection (Fig. 8c;

Table 8. Representative analyses of K-feldspar (24 oxygen basis)

Rock types	Sillimanite schist					
Metamorphic zone	Sillimanite zone					
Sample no.	SS1	SS1	SS1	SS1	SS1	SS1
Domain	R	C	C	R	R	C
SiO ₂	62.21	63.34	64.43	63.31	64.08	65.02
TiO ₂	0.03	0.02	0.01	0.02	0.01	0.02
Al ₂ O ₃	20.43	19.36	18.49	20.12	19.10	18.89
Cr ₂ O ₃	0.00	0.00	0.02	0.00	0.01	0.03
FeO	0.02	0.03	0.02	0.01	0.02	0.01
MnO	0.00	0.10	0.01	0.02	0.02	0.10
MgO	0.02	0.03	0.01	0.02	0.03	0.01
CaO	0.20	0.15	0.17	0.16	0.13	0.12
Na ₂ O	4.54	3.28	4.01	4.48	4.89	4.12
K ₂ O	12.56	13.67	12.79	11.80	11.50	11.70
Total	100.01	99.98	99.96	99.94	99.79	100.02
Si	2.87	2.93	2.96	2.91	2.94	2.97
Ti	0.00	0.00	0.00	0.00	0.00	0.00
Al	1.11	1.05	1.00	1.09	1.03	1.02
Cr	0.00	0.00	0.00	0.00	0.00	0.00
Fe	0.00	0.00	0.00	0.00	0.00	0.00
Mn	0.00	0.00	0.00	0.00	0.00	0.00
Mg	0.00	0.00	0.00	0.00	0.00	0.00
Ca	0.01	0.01	0.01	0.01	0.01	0.01
Na	0.41	0.29	0.36	0.40	0.44	0.36
K	0.74	0.81	0.75	0.69	0.67	0.68
Total	5.14	5.10	5.09	5.09	5.10	5.04
X _K	0.64	0.73	0.67	0.63	0.60	0.65

X_K = K/(Ca + Na + K); C - core; R - rim;

Grt = garnet, Bt = biotite, Ms = muscovite, Chl = chlorite, St = staurolite, Sil = sillimanite.

Table 9) at 5.4 kbar, 550 °C. Similarly, for the sillimanite zone, end-member phases used include albite, annite, beta-quartz, K-feldspar, paragonite, phlogopite, pyrope, sillimanite, staurolite and water. There are six possible equilibria that can be written for the selected end-member phases. Use of these equilibria for sample SS1 gives precise intersection (Fig. 8d; Table 9) at 6.4 kbar, 675 °C.

6.b. Phase equilibria modelling

The prograde metamorphic history of the schists in and around the Kandra area is constrained using various *P–T* pseudosections relevant to the mineral assemblages preserved in different rocks of the area. These pseudosections involve the use of the preferred bulk composition of rocks to predict the metamorphic mineral assemblages at equilibrium within a certain pressure–temperature window (Powell & Holland, 1988; Holland & Powell, 1998; White *et al.* 2001, 2003, 2007; Clark & Hand, 2010). The pseudosections have a major advantage over *P–T* petrogenetic

grids in that they portray and quantify multivariant equilibria. Respective stability fields of different mineral assemblages bounded by either univariant reaction lines or zero mode isopleths, at a range of *P–T* conditions, can be shown by phase equilibria modelling. The bulk rock compositions of the representative samples collected from the study area were analysed using X-ray fluorescence (XRF) technique (Siemens Sequential X-ray Spectrometer SRS 3000 (Wavelength Dispersive) at Wadia Institute of Himalayan Geology, Dehradun, India). The amount of H₂O used for *P–T* pseudosection calculations was approximated from the 'loss on ignition' (LOI) value obtained during XRF analysis. Based on the amounts of major oxides obtained from bulk rock analysis along with the calculated amount of H₂O, *P–T* pseudosections were constructed using Perple_X software (version 6.7.2). For the different metamorphic zones, different pseudosections have been constructed. The detailed formula, notation and sources of the solution models are given in Table 10. Based on the mineral assemblages and compositions, an 11-component system MnNCKFMASHTO (MnO–Na₂O–CaO–K₂O–FeO–MgO–Al₂O₃–SiO₂–H₂O–TiO₂–Fe₂O₃) was chosen for pseudosection construction.

The pressure range considered for the biotite zone is 2–6 kbar, and the temperature range is 327–627 °C; for the garnet zone the pressure ranges from 3 to 8 kbar, and temperature from 300 to 700 °C; for the staurolite zone, *P* and *T* values ranges respectively between 3 and 8 kbar and 300 and 900 °C; for the sillimanite zone, the pressure range between 4 and 8 kbar and temperature range between 427 and 827 °C were taken. The *P–T* conditions derived through X_{Mg} and X_{Ti} biotite (sample no. S5) intersect at 445 °C and 4.4 kbar for the biotite zone (Fig. 9a, b). The pseudosection (sample no. SG1) was contoured by X_{Mg} garnet and X_{Mg} biotite isopleths. The calculated isopleths intersect at 5 kbar and 540 °C for the garnet zone (Fig. 10a, b). The pseudosection (sample no. K13) is contoured by X_{Mg} garnet, X_{Mg} biotite and X_{Mg} staurolite isopleths. The calculated isopleths for X_{Mg} garnet and biotite intersect at 5.3 kbar and 550 °C for the staurolite zone (Fig. 11a, b). The pseudosection (sample No. SS1) was contoured by X_{Mg} garnet, X_{Mg} staurolite and X_{Mg} biotite isopleths. The calculated isopleths for X_{Mg} garnet and biotite intersect at 6.4 kbar and 675 °C for the sillimanite zone (Fig. 12a, b). *P–T* pseudosection calculations were constructed to model peak conditions for the present mineral assemblages. The calculation reliability is dependent on the uncertainties in effectual bulk composition (chemical refraction caused by the growth of garnet porphyroblast), fluid infiltration, partial melting and compositional zoning in the garnet (Tinkham & Ghent, 2005). Therefore, a small variation in both the whole-rock geochemistry and equilibrating *P–T* condition cannot be ruled out.

7. Discussion

7.a. *P–T* conditions of prograde metamorphic zones

The textural study of phyllites and schists has revealed a time relation between crystallization and deformation. Crystallization of biotite is earlier than garnet because the former constitutes the S₂ foliation and occurs as inclusion in garnet. Garnet precedes the formation of staurolite and has commonly a synkinematic core while staurolite is mostly later syn- to post-tectonic as evidenced by the parallelism of S₁ with S_e of S₂. In a few thin-sections, garnet with 'S'-shaped S₁ trails is in contact with staurolite with straight S₁ trails (Fig. 5c). Kyanite as such appears earlier well within the biotite

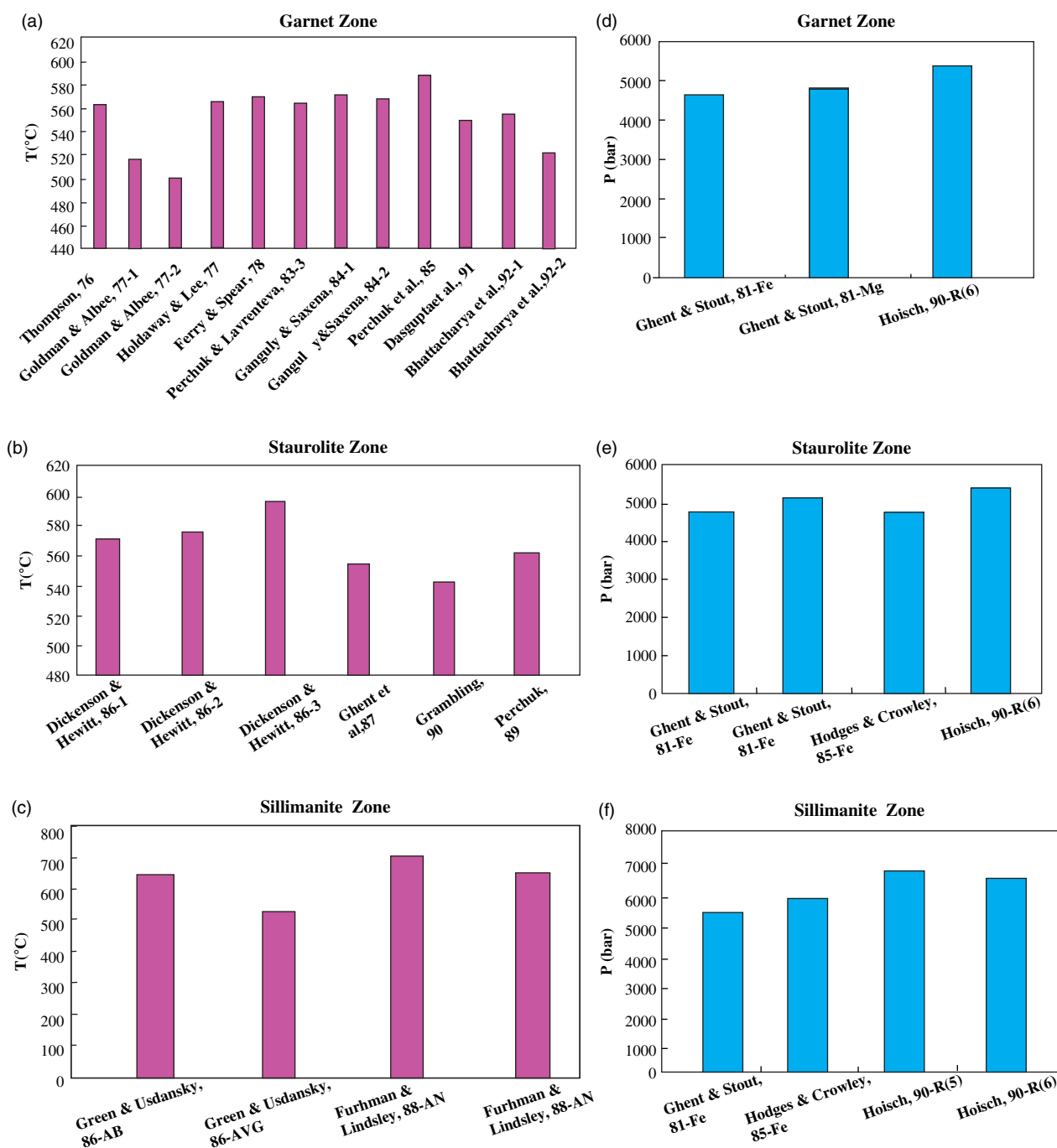


Fig. 7. (Colour online) (a) Coexisting garnet–biotite pairs (garnet zone) and derivative temperature (°C) at 5 kbar. (b) Coexisting garnet–chlorite pairs (stauroilite zone) and derivative temperature (°C) at 5.5 kbar. (c) Coexisting plagioclase – K-feldspar (sillimanite zone) pairs and derivative temperature (°C) at 6.5 kbar. (d) Coexisting garnet–plagioclase–biotite–muscovite–quartz assemblage (garnet zone) and derivative pressure (kbar) at 550 °C. (e) Coexisting garnet–plagioclase–biotite–muscovite–quartz assemblage (stauroilite zone) and derivative pressure (kbar) at 550 °C. (f) Coexisting garnet–plagioclase–biotite–muscovite–quartz assemblage (sillimanite zone) and derivative pressure (kbar) at 700 °C.

zone, but kyanite coexisting with staurolite shows textural feature indicating its crystallization later than staurolite, e.g. staurolite crystals are approximately aligned parallel to S_2 foliation while kyanite occurs as idioblastic to subidioblastic crystals cutting across the foliation. Similarly, sillimanite post-dates staurolite as it occurs with muscovite pseudomorphs after staurolite. The time relation between kyanite and sillimanite is not clear in the area on account of the sporadic occurrence of kyanite. Nevertheless, from the evidence of fibrolitization of kyanite, as mentioned by Roy (1966), it is evident that sillimanite started crystallization later than

kyanite. In the Kandra area, there is textural evidence of the close association of sillimanite with staurolite, and similarity of the mineral assemblages of staurolite–kyanite and sillimanite zones suggests the formation of sillimanite-bearing schists from pre-existing staurolite schists. The formation of garnet from chlorite–muscovite is not readily evident from the textural relation of the pelites of the garnet zone. However, retrogression of garnet to chlorite suggests that chlorite may have been involved. Similarly, partial retrogression of staurolite to chlorite and white mica probably indicates that staurolite may form by reactions involving

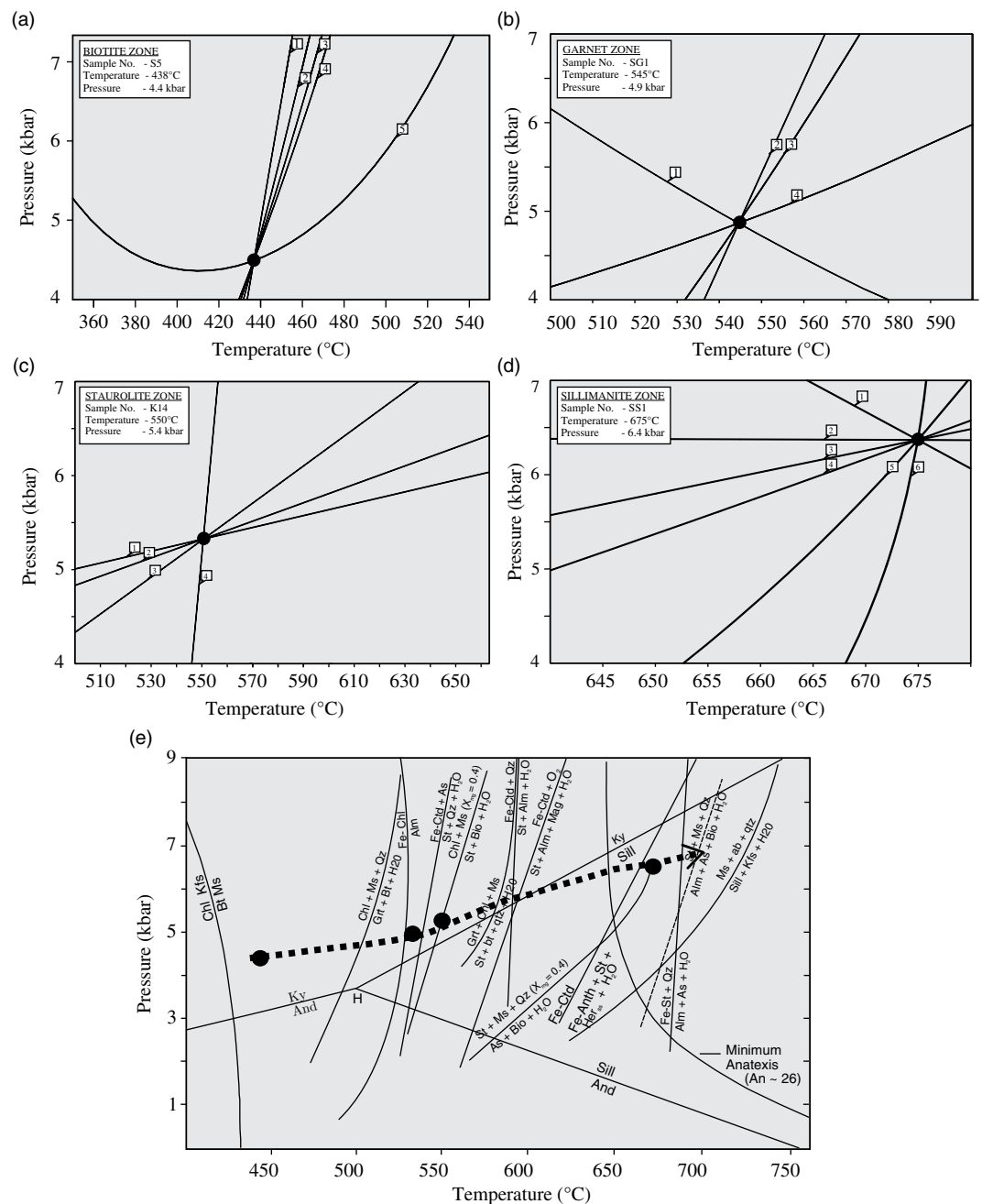


Fig. 8. Calculated P - T conditions for different zones obtained by application of the winTWQ program using the equilibria listed in Table 9. Schematic P - T grid illustrating the stability fields for different metamorphic zones of metamorphism. Calculated P - T values for different zones are shown by yellow solid circles. Al_2SiO_5 triple point and emerging univariant curves after Holdaway (1971). Anatexis minimum curve for plagioclase (An26) after Bucher & Grapes (2011). Different equilibria reactions are shown, as determined experimentally. The solid line with an arrow indicates the postulated P - T gradient during the prograde regional metamorphism.

chlorite and muscovite. It is also possible to reconcile that metamorphic reaction inferred to have been in progress by the comparison of the compatible mineral assemblages on either side of the isograd as shown in Figure 8e. As the reactions proceed, there is a gradual reduction and ultimate disappearance of one or more reactant minerals, compensated by the appearance and growth of product minerals. It is thus not surprising that textural evidence indicates that all the mineral assemblages of the higher-grade zones that have passed through low-grade zones mapped in space in the Kandra area correspond to the time sequence and can be reconciled with the metamorphic reactions inferred to have been in progress.

P - T pseudosections in relevant model systems have been constructed for different zones. The calculated isopleths in the above P - T pseudosections were corroborated with obtained

probe data of different mineral phases from these representative rock samples. The pressure and temperature conditions are estimated by comparing the natural assemblages and metamorphic reactions derived for each isograd with experimentally determined analogous mineral reactions, and through various models of mineral equilibria. Metamorphic conditions have been estimated using an internally consistent winTWQ program and Perple_X software in the MnNCKFMASHTO model system. The combination of these approaches suggests the following temperatures ($\pm 50^\circ\text{C}$) and pressures (± 0.5 kbar): 440 $^\circ\text{C}$ / 4.5 kbar for the biotite zone, 550 $^\circ\text{C}$ / 5.0 kbar for the garnet zone, 600 $^\circ\text{C}$ / 5.5 kbar for the staurolite zone and 675 $^\circ\text{C}$ / 6.5 kbar for the sillimanite zone.

For a characterization of the P - T regime during metamorphism, the garnetiferous lithologies are most suitable, since a set

Table 9. Simultaneous calculation of *P*–*T* by winTWQ program

Equilibria plotted in Fig. 7a dS dV	
Biotite zone: (J K ⁻¹)(J bar ⁻¹)	
1	2 Hm + Qtz + Sd = Ms + 2 Mt – 19.68 – 0.49
2	8 Ann + 3 Chl + 9 Ms = 12 Sd + 21 Qtz + 6 Phl + 12 H ₂ O – 84.03 – 8.8
3	2 Ann + 2 Chl + 6 Ms = 3 Sd + 14 Qtz + 6 Eas + 8 H ₂ O – 147.16 – 5.75
4	2 Ann + Chl + 6 Hm = 4 Qtz + Phl + 6 Mt + Eas + 4 H ₂ O – 105.27 – 4.40
5	8 Ann + 3 Chl + 42 Hm + 9 Sd = 5 Phl + 12 Ms + 42 Mt + 12 H ₂ O – 497.23 – 19.20
Equilibria plotted in Fig. 7b	
Garnet zone:	
1	3 Chl + 6 Ky + 24 Mt + 12 Kfs = 5 Py + 4 Ms + 24 Hm + 8 Ann 78.89 – 17.72
2	3 Chl + 4 Gr + 30 Ky + 4 Phl = 9 Py + 4 Ms + 12 Mrg 684.047.85
3	Alm + 3 Hm + Phl = Py + Kfs + 3 Mt + H ₂ O – 6.38 – 0.024
4	2 Ann + Gr + 6 Hm + 6 Ky + Phl = Py + 3 Kfs + 3 Mrg + 6 Mt 151.29 6.399
Equilibria plotted in Fig. 7c	
Staurolite zone:	
1	6 St + 32 Py + 32 Kfs + 39 Gr + 20 H ₂ O = 8 Alm + 117 An + 32 P 19.919 0.329
2	6 St + 24 Py + 32 Kfs + 39 Gr + 20 H ₂ O = 8 Ann + 117 An + 24 Phl – 1567.19 – 92.84
3	6 St + 32 Kfs + 39 Gr + 24 Alm + 20 H ₂ O = 32 Ann + 117 An 646.83 94.13
4	Phl + Alm = Ann + Py – 814.64 – 44.17
Equilibria plotted in Fig. 7d	
Sillimanite zone:	
1	8 Ann + 29 Pg + 17 Kfs + 25 Py = 6 St + 30 Qtz + 25 Phl + 29 Ab – 227.00 29.70
2	8 Ann + 39 Pg + 7 Kfs + 15 Py = 6 St + 15 Phl + 39 Ab + 20 H ₂ O – 672.24 – 0.94
3	46 Ab + 8 Phl + 6 St + 34 H ₂ O = 21 Qtz + 8 Py + 46 Pg + 8 Ann 983.91 22.39
4	8 Ann + 54 Pg + 45 Qtz = 6 St + 8 Kfs + 54 Ab + 50 H ₂ O – 1340.12 – 46.90
5	Gr + Qtz + 2 Sil = 3An – 44.52 – 3.06
6	8 Ann + 46 Kfs + 54 Py + 58 H ₂ O = 6 St + 117 Qtz + 54 Phl 1223.51 121.13

Phases used in calculation: Ab, albite; Alm, almandine; An, anorthite; Ann, annite; Chl, chlorite; Eas, eastonite; Gr, grossular; Hm, hematite; Kfs, k-feldspar; Ky, kyanite; Mrg, margarite; Ms, muscovite; Mt, magnetite; Pg, paragonite; Phl, phlogopite; Py, pyrope; Qtz, beta-quartz; Sd, siderite; Sil, sillimanite; St, staurolite; dS and dV are calculated at 1 bar and 298 K.

of reasonably well-calibrated geothermobarometers based on pressure-sensitive net-transfer reactions and Fe–Mg exchange equilibria are available. Application of thermobarometry is plagued by a number of important factors that contribute as sources of error, e.g. re-equilibrium during retrogression, quality of thermobarometric formulations, extrapolations, restraints and sensitivity of thermometers, analytical errors in microprobe data, effect of other components in solid solutions, effect of cation order/disorder, error analyses and blocking effect (Spear, 1993). The temperatures calculated using the winTWQ program and pseudosection modelling compare well with those obtained from conventional thermobarometry (Figs 7, 8). The yielded differences are 0.3–0.9 kbar in pressure values for PMg and PFe, respectively. Such variation in absolute pressure values could be related to the uncertainties associated with thermochemical data in locating the end-member reactions.

7.b. Mechanisms for metamorphic zones

Due to the absence of top and bottom criteria, no relation has been established between the metamorphism and stratigraphic depth (Sarkar & Saha, 1977; Bhattacharya & Sanyal, 1988). So far as the relation with tectonic depth is concerned, the lower-grade rocks occupy shallower tectonic level towards the directions of axial plunge and in the flanks of the geanticlinorium of Dunn (1929) and Dunn & Dey (1942), later termed Singhbhum anticlinorium by Sarkar & Saha (1962). The higher-grade rocks occur at deeper tectonic levels away from the plunge direction towards the region of axial culmination (Naha, 1965; Matin *et al.* 2012). It is worth mentioning here that the transposition of planar fabric at hinge zones has been noticed in the study area near the bank of Sanjay river in Parbatipur (Fig. 3a). It is a significant signature of intense shearing. The general straight trend of the isograd in the NSMB may be correlated with very low plunge (Naha, 1965; Ray & Gangopadhyay, 1971; Banerjee & Matin, 2013).

Turner (1968) suggested that temperature corresponding to the amphibolite and granulite facies could not be maintained at levels above 50–80 km by burial alone. In accordance with Turner (1968), Kent (1991) and Mahato *et al.* (2008), the heat flow during regional metamorphism of the Kandra area might have been much higher than the 'normal' value of 10–15 °C km⁻¹. James (1955) and Ray *et al.* (2003) have calculated geothermal gradients based on the assumption that the metamorphic isograds are on the order of 100 °C apart and therefore indicate a gradient of 70 to 130 °C km⁻¹. The higher the magnitude of the heat flow, the greater is the rise of temperature with increasing depth. According to Ray *et al.* (2003) and Bucher & Grapes (2011), in many areas the geothermal gradient accounts for 60 °C km⁻¹ within the uppermost few kilometres of depth. However, in other areas (Jones, 1988; Drury, 1991), e.g. the Hungarian basin, the geothermal gradient is *c.* 54 °C km⁻¹ or as much as 100 °C km⁻¹ (Dövényi *et al.* 1983). Furthermore, there is broad localization in the form of elongate high-temperature zones along the axes of the Singhbhum metamorphic belt. There must be some mechanism for the localization of metamorphic heat. The direction of elongation of higher-temperature zones in the Singhbhum region is generally parallel to the fold axis of the geanticlinorium, and thus anisotropic heat conduction could account for this pattern. Many geologists have attributed it to granite intrusion or migmatization (Brown, 1994, 2001a). The stabilization of M₁ and M₂ phases, low-temperature influx during M₁, crustal loading during M₂ and the tectonic framework of the study area are very much suggestive of a clockwise prograde *P*–*T* path (England & Thomson, 1984). Authors are of the opinion in the light of the above discussion that the granites and the migmatites might have been the ultimate products of high-grade metamorphism (M₂ phase) rather than the cause of metamorphism as suggested by Brown (2001b) and, Brown & Sawyer (2008).

The development and evolution of the NSMB could be ideated best based on the ensialic orogenesis model (Fig. 13) (Kröner, 1979, 1981) of mobile belts or fold belts progression. Other tectonic models accounted in the formation of mobile belts are the back-arc marginal basin (Bose & Chakraborti, 1981), intraplate subduction (Sarkar & Saha, 1977) and micro-continental subduction models (Sarkar, 1982). The concept of Enisialic orogeny abides by the non-uniformitarian process (Windley, 1977) and stands eccentrically as a concept glided to Proterozoic plate tectonics. The connotation of initial rifting (initial phase of ensialic development) (Fig. 13a) and heat course from mantle upwelling sufficient for the M₁ metamorphism leading to the materialization of greenschist facies at low pressure, prior to orogeny (Robinson *et al.* 1999). The

Table 10. Solution notation, formula and model sources for phase

Symbols in Perple_X solution model file	Symbols used in drawn pseudosections	Solutions name	Formula	Source
Bi(W)	Bi	Biotite	$K[Mg_xFe_yMn_{1-x-y}]_{3-2w}Al_{1+2w}Si_{3-w}O_{10}(OH)_2, x + y \leq 1$	White <i>et al.</i> 2014
Gt(JH)	Grt	Garnet	$Fe_{3x}Ca_{3y}Mg_{3z}Mn_{3(1-x-y-z)}Al_2Si_3O_{12}, x + y + z \leq 1$	Jennings & Holland, 2015
Grt(W)	Grt	Garnet	$Fe_{3x}Ca_{3y}Mg_{3z}Mn_{3(1-x-y-z)}Al_2Si_3O_{12}, x + y + z \leq 1$	White <i>et al.</i> 2014
Chl(W)	Chl	Chlorite	$[Mg_xFe_wMn_{1-x-w}]_{5-y+z}Al_{2(1+y-z)}Si_{3-y+z}O_{10}(OH)_8, x + w \leq 1$	White <i>et al.</i> 2014
Mica(W)	Mica	Muscovite	$K_yCa_xNa_{1-x-y}(Mg_{1/2}Fe_{1/2})_wMg_wTi_wAl_{3+x-w-z}Si_{3-x+z}O_{10}(OH)_2, x + y \leq 1, w + z \leq y$	White <i>et al.</i> 2014
St(W)	St	Staurolite	$Mg_{4x}Fe_{4y}Mn_{4(1-x-y)}Al_{18}Si_{7.5}O_{48}H_{44}, x + y \leq 1$	White <i>et al.</i> 2014
Ctd(W)	Ctd	Chloritoid	$Mg_xFe_yMn_{1-x-y}Al_2SiO_5(OH)_2, x + y \leq 1$	White <i>et al.</i> 2014
melt(W)	melt	Melt	Na–Mg–Al–Si–K–Ca–Fe hydrous silicate melt	White <i>et al.</i> 2014
Pl(JH)	Ab, An	Plagioclase feldspar	$K_yNa_xCa_{1-x-y}Al_{2-x-y}Si_{2+x+y}O_8, x + y \leq 1$	Jennings & Holland, 2015
FspC1(W)	An, San, Abh	Ternary feldspar	$K_yNa_xCa_{1-x-y}Al_{2-x-y}Si_{2+x+y}O_8, x + y \leq 1$	White <i>et al.</i> 2014
Ilm(W)	Ilm	Ilmenite	$Mg_xMn_yFe_{1-x-y}TiO_3, x + y \leq 1$	White <i>et al.</i> 2014

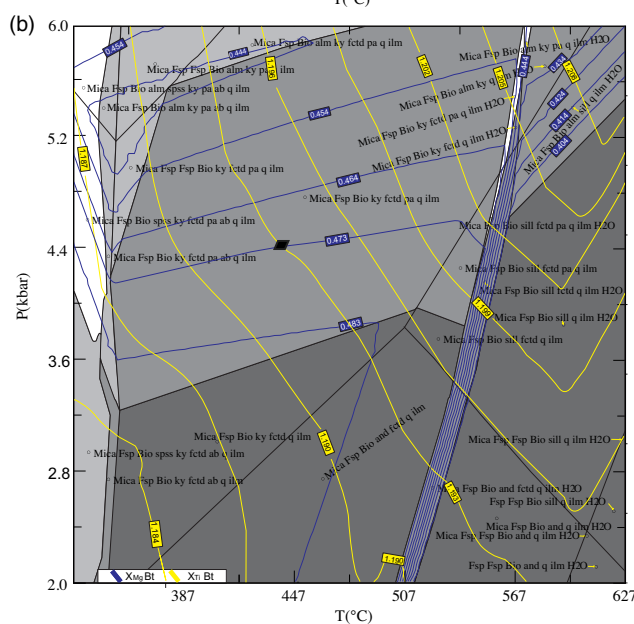
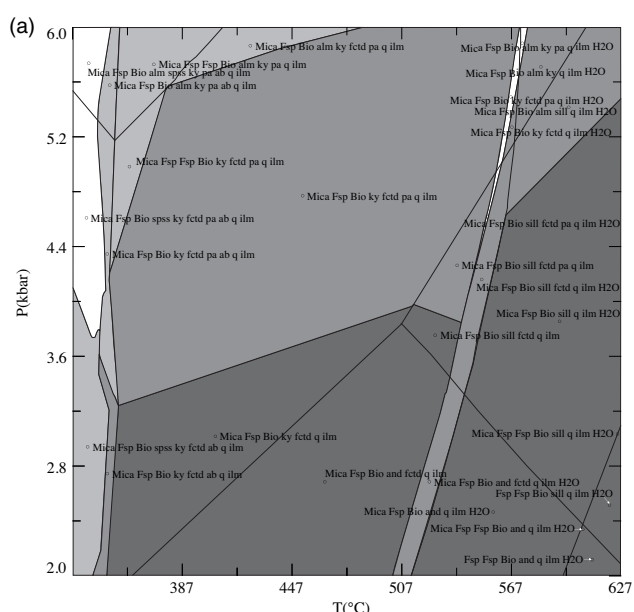


Fig. 9. (Colour online) (a) Calculated P – T pseudosection for biotite schist (sample no. S5) in the MnNCKFMASHTO system. Bulk composition in wt % (Na₂O 3.04, CaO 2.23, K₂O 4.41, FeO 7.38, Fe₂O₃ 0.92, MgO 3.47, Al₂O₃ 25.22, SiO₂ 49.17, H₂O 1.76, TiO₂ 0.82, H₂O 2.45, MnO 0.06). (b) The pseudosection has been contoured for the isopleths X_{Mg} and X_{Tl} . P – T condition obtained using biotite composition by the intersection of X_{Mg} and X_{Tl} .

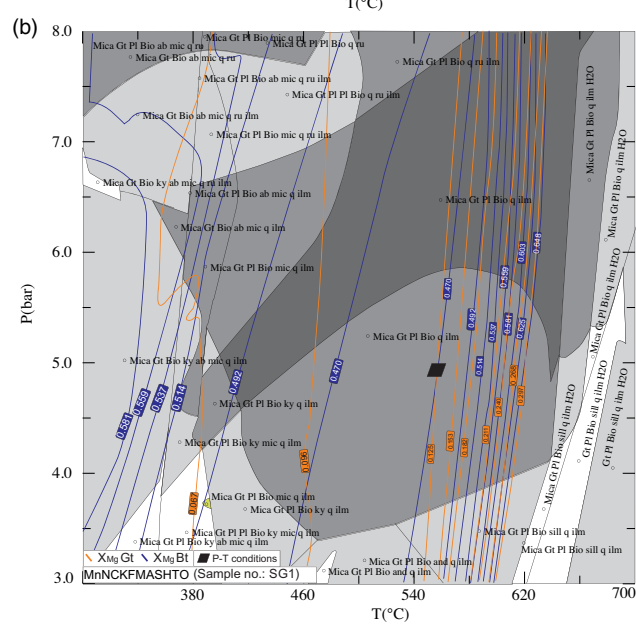
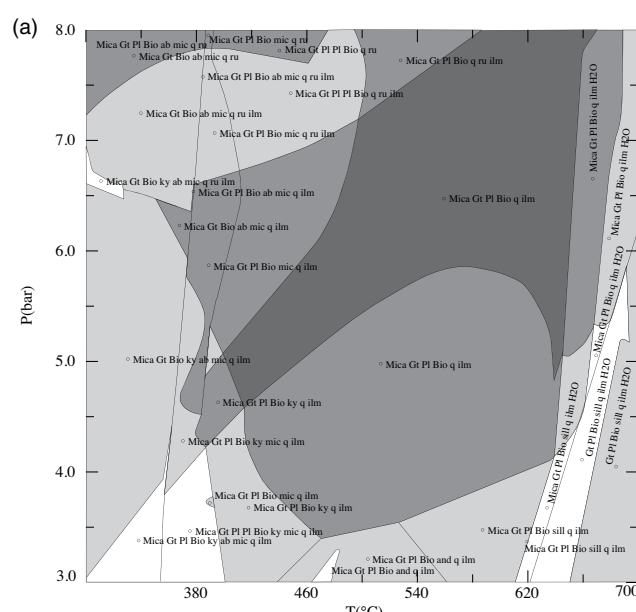


Fig. 10. (Colour online) (a) Calculated P – T pseudosection for garnet–biotite–muscovite schist (sample no. SG1) in the MnNCKFMASHTO system. Bulk composition in wt % (Na₂O 1.63, CaO 1.39, K₂O 1.23, FeO 3.28, Fe₂O₃ 0.41, MgO 1.78, Al₂O₃ 20.44, SiO₂ 60.32, H₂O 2.06, TiO₂ 0.86, MnO 0.19). (b) The pseudosection has been contoured for the isopleths X_{Mg} garnet and X_{Mg} biotite. P – T condition obtained using the intersection of X_{Mg} (garnet) and X_{Mg} (biotite).

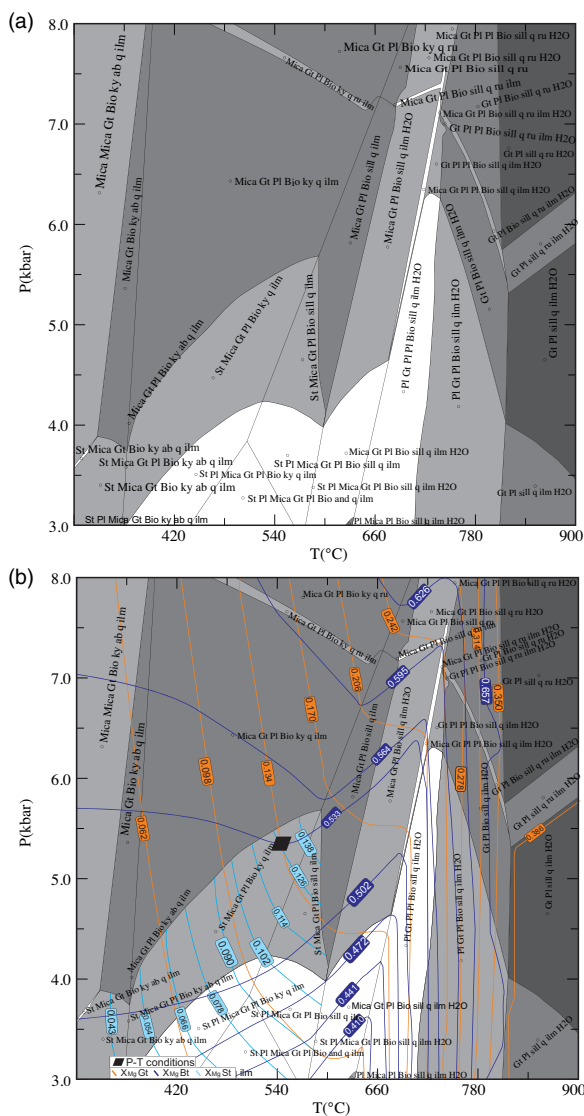


Fig. 11. (Colour online) (a) Calculated P - T pseudosection for garnet-staurolite-mica schist (sample no. K13) in the MnNCKFMASHTO system. Bulk composition in wt % (Na_2O 1.17, CaO 0.49, K_2O 3.73, FeO 3.28, Fe_2O_3 0.41, MgO 3.22, Al_2O_3 20.33, SiO_2 57.09, H_2O 1.76, MnO 0.07, TiO_2 1.03, H_2O 1.46). (b) The pseudosection has been contoured for the isopleths X_{Mg} garnet, X_{Mg} biotite and X_{Mg} staurolite. P - T condition obtained using the intersection of X_{Mg} (garnet) and X_{Mg} (biotite).

development of M_2 phase metamorphic facies could be envisioned by the lower crust heating and ductile shearing leading to delamination followed by gravitational instability of the subcrustal lithosphere which proffered sinking and subduction of the dense continental lithosphere (Fig. 13b). The field evidences for the required intense shearing responsible for the deformation D_2 and M_2 episode of metamorphism have been noticed in the form of dextrally rotated euhedral garnet porphyroblast (Fig. 4f) and transposition of planar fabric at hinge zones (Fig. 3a). In progression to this, the intracontinental orogeny entailing thrusting and nappe (Fig. 13c) tectonics, developed due to the action of differential stresses acting between the negatively buoyant inherent mantle lithosphere and less dense continental crust (Molnar & Gray, 1979), explains the D_1 and D_2 deformations and generation of M_2 metamorphic facies. We hereby interpret the event of M_2 metamorphism to be the main phase of metamorphism taking place post- D_1 and during late to post- D_2 . The thermodynamic establishment of the M_2 phase of metamorphism

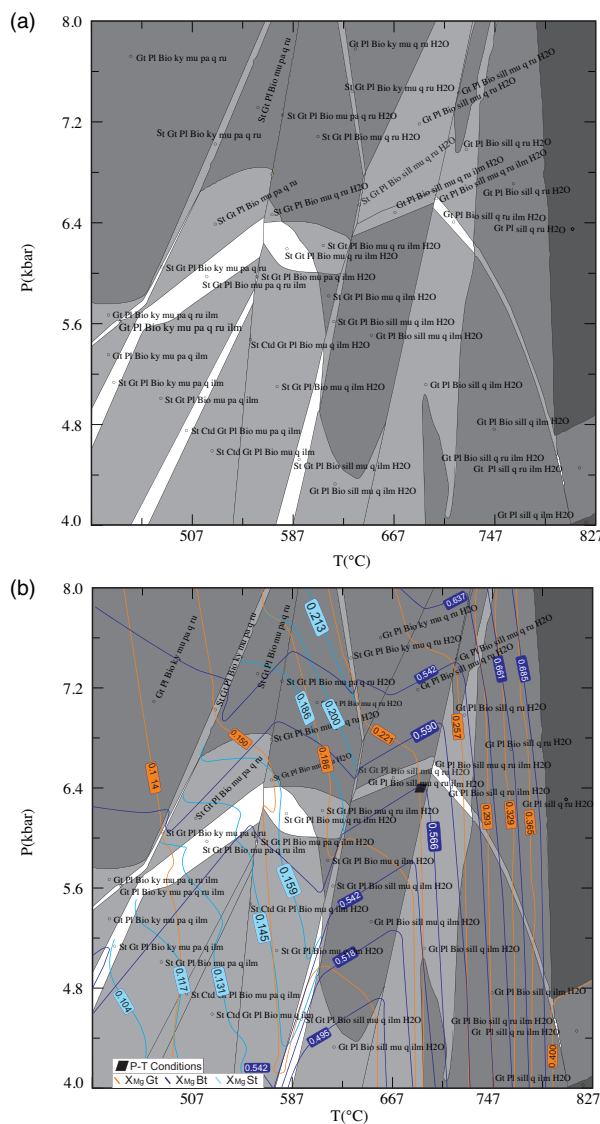


Fig. 12. (Colour online) (a) Calculated P - T pseudosection for sillimanite schist (sample no. SS1) in the MnNCKFMASHTO system. Bulk composition in wt % (Na_2O 1.88, CaO 0.98, K_2O 4.84, FeO 5.57, Fe_2O_3 0.70, MgO 2.32, Al_2O_3 24.33, SiO_2 55.39, H_2O 1.76, TiO_2 1.03, H_2O 2.22, MnO 0.1). (b) The pseudosection has been contoured for the isopleths X_{Mg} garnet, X_{Mg} biotite and X_{Mg} staurolite. P - T condition obtained using the intersection of X_{Mg} (garnet) and X_{Mg} (biotite).

could be well understood by the presence of staurolite, kyanite and garnet porphyroblasts (amphibolite facies) in a way that post-orogenesis the increase in crustal thickness (pressure implication) led to an increase in the radioactive heating which was imbued with frictional heating, providing the vital pressure and temperature conditions for metamorphism to take place.

8. Conclusions

The spatial distribution of the index minerals in the pelitic schists of the area shows Barrovian type of metamorphism. The different isograds delineated by the first appearance of index minerals are biotite, garnet, staurolite and sillimanite. The pressure and temperature conditions of metamorphism have been delineated by comparing the natural assemblages with the experimental data on the stability of minerals which indicate that metamorphism took

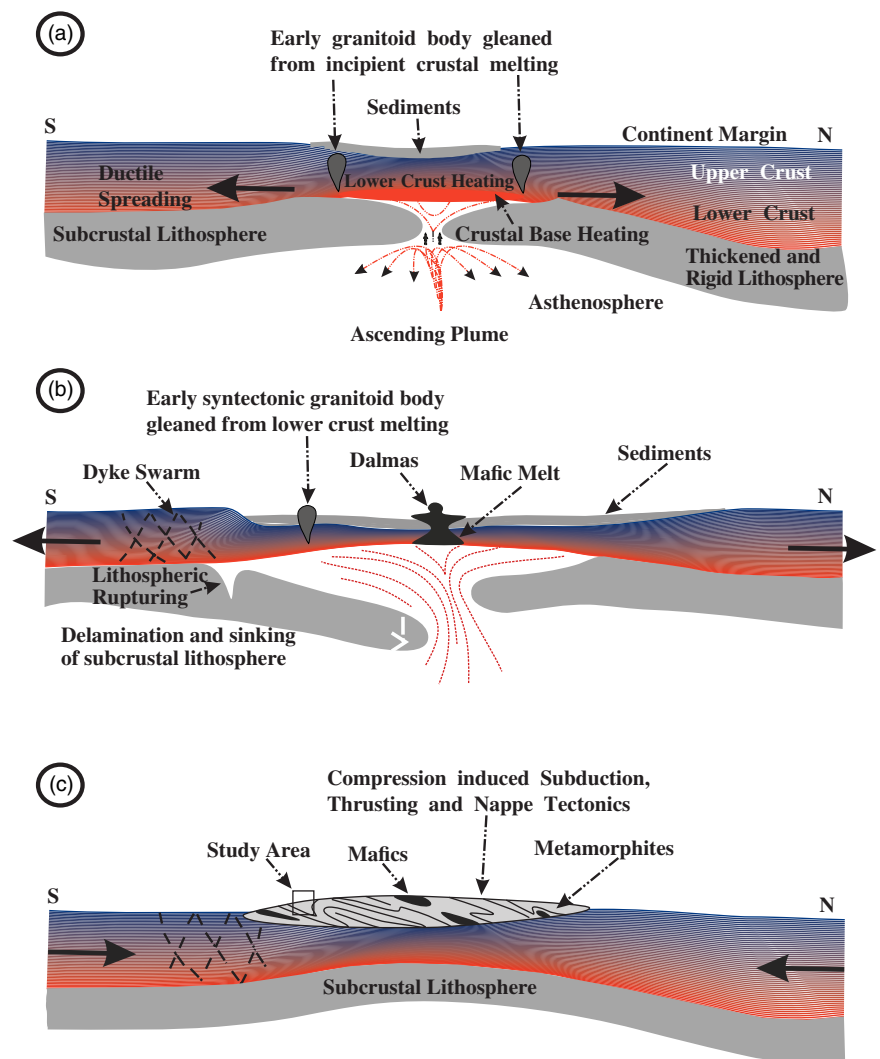


Fig. 13. (Colour online) Schematic representation of the tectonic evolution of the North Singhbhum Mobile Belt (NSMB) with delineation of the study area depicting ensialic origin (modified after Kröner, 1981).

place between >400 °C and 675 °C and at 4.5 to 6.5 kbar. In the study area, the gneisses are associated with biotite and garnet zones, therefore not spatially related to the high-grade sillimanite zone. Furthermore, it is considered by many petrologists that these gneisses are emplaced at a later time, during the waning phase of progressive metamorphism when the enveloping rocks were in a metamorphic condition corresponding to the lower greenschist facies, and thus no causal connection between gneisses and regional metamorphism exists since they are not synchronous in time. Thus, for the regional metamorphism in the study area, it may be necessary to assume an abnormally high rate of heat flow from the underlying basement extending to the mantle to provide heat for the metamorphism and the barrovian type of metamorphism differentiated in two phases, viz. M_1 and M_2 , facilitated by the upwelling asthenosphere and crustal loading (post-orogeny) acting as the heat source for M_1 and M_2 phases respectively. Besides metamorphic events in the study area, two deformation events (D_1 and D_2) in association with the development of two tectonic fabrics (S_2 and S_3), where the M_1 event dates pre- S_2 and pre- D_1 whereas M_2 is syn- S_3 and late to post- D_2 could be well understood.

Acknowledgements. This work has been possible through DST-SERB research project (P-07/704) to D.P. and a JRF (CSIR) to D.K.P. We also thank Head, Department of Geology, Banaras Hindu University and the CAS programme of the UGC at BHU for providing necessary infrastructural facilities. Anonymous reviewers are thanked for constructive comments.

References

- Acharyya SK, Gupta A and Orihashi Y (2010) Neoproterozoic-Palaeoproterozoic stratigraphy of the Dhanjori basin, Singhbhum Craton, eastern India: and recording of a few U-Pb zircon dates from its basal part. *Journal of Asian Earth Science* **39**, 527–36.
- Banerjee S and Matin A (2013) Evolution of microstructures in Precambrian shear zones: an example from eastern India. *Journal of Structural Geology* **50**, 199–208.
- Berman RG (1988) Internally-consistent thermodynamic data for minerals in the system $\text{Na}_2\text{O}-\text{K}_2\text{O}-\text{CaO}-\text{MgO}-\text{FeO}-\text{Fe}_2\text{O}_3-\text{Al}_2\text{O}_3-\text{SiO}_2-\text{TiO}_2-\text{H}_2\text{O}-\text{CO}_2$. *Journal of Petrology* **29**, 445–522.
- Berman RG (1991) Thermobarometry using multi-equilibrium calculations; a new technique, with petrological applications. *The Canadian Mineralogist* **29**, 833–55.
- Berman RG and Aranovich LY (1996) Optimized standard state and mixing properties of minerals: I. model calibration for olivine, orthopyroxene, cordierite, garnet, and ilmenite in the system $\text{FeO}-\text{MgO}-\text{CaO}-\text{Al}_2\text{O}_3-\text{TiO}_2-\text{SiO}_2$. *Contributions to Mineralogy and Petrology* **126**, 1–24.
- Bhattacharya A, Mohanty L, Maji A, Sen SK and Raith M (1992) Non-ideal mixing in the phlogopite-annite binary: constraints from experimental data on Mg-Fe partitioning and a reformulation of the biotite-garnet geothermometers. *Contributions to Mineralogy and Petrology* **111**, 87–93.
- Bhattacharya DS and Sanyal P (1988) The Singhbhum orogeny – its structure and stratigraphy. *Memoirs of the Geological Survey of India* **8**, 85–111.
- Bhattacharya HN, Nelson DR, Thern ER and Altermann W (2014) Petrogenesis and geochronology of the Arkasani Granophyre and felsic

- Dalma volcanic rocks: implications for the evolution of the Proterozoic North Singhbhum Mobile Belt, east India. *Geological Magazine* **152**, 492–503.
- Bose MK and Chakraborti MK** (1981) Fossil marginal basin from the Indian shield: a model for the evolution of the Singhbhum Precambrian belt, eastern India. *Geologische Rundschau* **70**, 514–18.
- Brown M** (1994) The generation, segregation, ascent and emplacement of granite magma: the migmatite-to-crustally-derived granite connection in thickened orogens. *Earth-Science Reviews* **36**, 83–130.
- Brown M** (2001a) Crustal melting and granite magmatism: key issues. *Physics and Chemistry of the Earth, Part A: Solid Earth and Geodesy* **26**, 201–12.
- Brown M** (2001b) Orogeny, migmatites and leucogranites: a review. *Journal of Earth System Science* **110**, 313–36.
- Brown M and Sawyer EW** (2008) Granites, migmatites and residual granulites: relationships and processes. In *Working with Migmatites* (eds EW Sawyer and M Brown), pp. 97–144. Quebec City: Mineralogical Association of Canada Short Course Series 38.
- Bucher K and Grapes R** (2011) Metamorphism of dolomites and limestones. In *Petrogenesis of Metamorphic Rocks*, pp. 225–55. Berlin and Heidelberg: Springer.
- Chakraborty KR and Sen SK** (1967) Regional metamorphism of pelitic rocks around Kandra, Singhbhum, Bihar. *Contributions to Mineralogy and Petrology* **16**, 210–32.
- Chakraborty M, Sengupta N, Biswas S and Sengupta P** (2015) Phosphate minerals as a recorder of P-T-fluid regimes of metamorphic belts: example from the Palaeoproterozoic Singhbhum Shear Zone of the East Indian shield. *International Geology Review* **57**, 1619–32.
- Clark C and Hand M** (2010) Decoding Mesoproterozoic and Cambrian metamorphic events in Willyama Complex metapelites through the application of Sm-Nd garnet geochronology and P-T pseudosection analysis. *Gondwana Research* **17**, 59–74.
- Dasgupta S, Sengupta P, Guha D and Fukuoka M** (1991) A refined garnet-biotite Fe-Mg exchange geothermometer and its application in amphibolites and granulites. *Contributions to Mineralogy and Petrology* **109**, 130–7.
- Dickenson MP and Hewitt DA** (1986) A garnet-chlorite geothermometer. *Geological Society of America Abstracts with Programs* **18**, 584.
- Dövényi P, Horváth F, Liebe P, Gálfi J and Erki I** (1983) Geothermal conditions of Hungary. *Geophysical Transactions* **29**, 3–114.
- Drury MJ** (1991) Heat flow in the Canadian Shield and its relation to other geophysical parameters. In *Terrestrial Heat Flow and the Lithosphere Structure*, pp. 317–37. Berlin and Heidelberg: Springer.
- Dunn JA** (1929) The geology of north Singhbhum including parts of Ranchi and Manbhum districts. *Memoirs of the Geological Survey of India* **54**, 166 pp.
- Dunn JA and Dey AK** (1942) The geology and petrology of eastern Singhbhum and surrounding areas. *Memoirs of the Geological Survey of India* **69**, 281–450.
- Dwivedi SB and Lal SN** (1992) Prograde Barrovian type of metamorphism of pelitic rocks around Kandra, District Singhbhum, Bihar. *Proceedings - Indian National Science Academy, Part A* **58**, 195–206.
- Dwivedi SB, Singh TN and Prakash D** (1993) Precambrian metamorphites of the area around Kandra, district Singhbhum, Bihar. *Indian Journal of Engineers* **23**, 83–8.
- England PC and Thomson AB** (1984) Pressure-temperature-time paths of regional metamorphism I. Heat transfer during the evolution of regions of thickened continental crust. *Journal of Petrology* **25**, 894–928.
- Eriksson PG, Mazumder R, Cataneanu O, Bumby AJ and Ilondo B** (2006) Precambrian continental freeboard and geological evolution: a time perspective. *Earth Science Review* **79**, 165–204.
- Eriksson PG, Mazumder R, Sarkar S, Bose PK, Altermann W and Van der Merwe R** (1999) The 2.7–20 Ga volcano-sedimentary record of Africa, India and Australia: evidence for global and local changes in sea level and continental freeboard. *Precambrian Research* **97**, 269–302.
- Ferry JM and Spear FS** (1978) Experimental calibration of the partitioning of Fe and Mg between biotite and garnet. *Contributions to Mineralogy and Petrology* **66**, 113–17.
- Fuhrman ML and Lindsley DH** (1988) Ternary-feldspar modeling and thermometry. *American Mineralogist* **73**, 201–15.
- Ganguly J and Saxena SK** (1984) Mixing properties of aluminosilicate garnets: constraints from natural and experimental data, and applications to geothermobarometry. *American Mineralogist - Mineralogical Society of America* **69**, 88–97.
- Ghent ED and Stout MZ** (1981) Geothermometry and geobametry of plagioclase-biotite-garnet-muscovite assemblages. *Contributions to Mineralogy and Petrology* **76**, 92–7.
- Ghent ED, Stout MZ, Black PM and Brothers RN** (1987) Chloritoid-bearing rocks associated with blueschists and eclogites, northern Caledonia. *Journal of Metamorphic Geology* **5**, 239–54.
- Goldman AE and Albee AL** (1977) Correction of Mg/Fe partitioning between garnet and biotite with 18O/16O partitioning between quartz and magnetite. *American Journal of Science* **277**, 750–67.
- Grambling JA** (1990) Internally-consistent geothermometry and H₂O barometry in metamorphic rocks: the example garnet-chloride-quartz. *Contributions to Mineralogy and Petrology* **105**, 617–28.
- Green NL and Usdansky SI** (1986) Ternary-feldspar mixing relations and thermobarometry. *American Mineralogist - Mineralogical Society of America* **71**, 1100–8.
- Guidotti CV** (1970) The mineralogy and petrology of the transition from the lower to upper sillimanite zone in the Oquossoc area, Maine. *Journal of Petrology* **11**, 277–336.
- Henry DJ, Guidotti CV and Thomson JA** (2005) The Ti-saturation surface for low-to-medium pressure metapelitic biotites: implications for geothermometry and Ti-substitution mechanisms. *American Mineralogist* **90**, 316–28.
- Hodges KV and Crowley PD** (1985) Error estimation and empirical geothermobarometry for pelitic systems. *American Mineralogist - Mineralogical Society of America* **70**, 702–9.
- Hoisch TD** (1990) Empirical calibration of six geobarometers for the mineral assemblage quartz + muscovite + biotite + plagioclase + garnet. *Contributions to Mineralogy and Petrology* **104**, 225–34.
- Holdaway MJ** (1971) Stability of andalusite and the aluminium silicate phase diagram. *American Journal of Sciences* **271**, 97–131.
- Holdaway MJ and Lee SM** (1977) Fe-Mg cordierite stability in high grade pelitic rocks based on experimental, theoretical and natural observations. *Contributions to Mineralogy and Petrology* **6**, 175–98.
- Holland TJB and Powell RTJB** (1998) An internally consistent thermodynamic data set for phases of petrological interest. *Journal of Metamorphic Geology* **16**, 309–43.
- Iyengar SVP and Murthy YGK** (1982) The evolution of the Archean-Proterozoic crust in parts of Bihar and Orissa, eastern India. *Records of the Geological Survey of India* **112**, 1–5.
- James HL** (1955) Zones of regional metamorphism in the Precambrian of northern Michigan. *Geological Society of America Bulletin* **66**, 1455–88.
- Jennings ES and Holland TJB** (2015) A simple thermodynamic model for melting of peridotite in the system NCFMASOCr. *Journal of Petrology* **56**, 869–92.
- Jones MQW** (1988) Heat flow in the Witwatersrand Basin and environs and its significance for the South African shield geotherm and lithosphere thickness. *Journal of Geophysical Research: Solid Earth* **93**, 3243–60.
- Kent R** (1991) Lithospheric uplift in eastern Gondwana: evidence for a long-lived mantle plume system? *Geology* **19**, 19–23.
- Kröner A** (1979) Pan African plate tectonics and its repercussions on the crust of northeast Africa. *Geologische Rundschau* **68**, 565–83.
- Kröner A** (1981) Precambrian plate tectonics. In *Precambrian Plate Tectonics*, vol. 4 (ed A Kröner), pp. 57–90. Amsterdam: Elsevier.
- Lal RK, Ackermann D and Singh JB** (1987) Geothermobarometry in Barrovian type of metamorphism of pelitic schists, Sini, district Singhbhum. *Recent Researches in Geology* **13**, 125–42.
- Lal RK and Singh JB** (1978) Prograde polyphase regional metamorphism and metamorphic reactions in pelitic schists at Sini, district Singhbhum, India. *Neues Jahrbuch für Mineralogie* **131**, 304–33.
- Mahadevan TM** (2002) *Geology of Bihar and Jharkhand*. Bangalore: Geological Society of India, 563 pp.
- Mahato S, Goon S, Bhattacharya A, Mishra B and Bernhardt HJ** (2008) Thermo-tectonic evolution of the North Singhbhum Mobile Belt (eastern

- India): a view from the western part of the belt. *Precambrian Research* **162**, 102–27.
- Matin A, Banerjee S, Gupta CD and Banerjee N** (2012) Progressive deformation across a ductile shear zone: an example from the Singhbhum Shear Zone, eastern India. *International Geology Review* **54**, 290–301.
- Mazumder R** (2005) Proterozoic sedimentation and volcanism in the Singhbhum crustal province, India and their implications. *Sedimentary Geology* **176**, 167–93.
- Mazumder R, Bose PK and Sarkar S** (2000) A commentary on the tectono-sedimentary record of the pre-2.0 Ga continental growth of India vis-a-vis pre-Gondwana Afro-Indian supercontinent. *Journal of African Earth Science* **30**, 201–17.
- Mazumder R, Van Loon AJ, Mallik L, Reddy SM, Arima M, Altermann W, Eriksson PG and De S** (2012a) *Mesoarchaean-Palaeoproterozoic stratigraphic record of the Singhbhum crustal province, eastern India: A synthesis*. In *Palaeoproterozoic of India* (eds R Mazumder and D Saha), pp. 31–49. Geological Society of London, Special Publication no. 365.
- Mazumder R, Eriksson PG, De S, Bumby AJ and Lenhardt N** (2012b) Palaeoproterozoic sedimentation on the Singhbhum craton: global context and comparison with Kaapvaal. In *Palaeoproterozoic of India* (eds R Mazumder and D Saha), pp. 51–76. Geological Society of London, Special Publication no. 365.
- Mitra R** (1954) Pelitic metamorphites around Kandra, Singhbhum. *Quarterly Journal of the Geological, Mining and Metallurgical Society of India* **26**, 149–68.
- Molnar P and Gray D** (1979) Subduction of continental lithosphere: some constraints and uncertainties. *Geology* **7**, 58–62.
- Mukhopadhyay D** (2001) The Archaean nucleus of Singhbhum: the present state of knowledge. *Gondwana Research* **4**, 307–18.
- Naha K** (1961) Precambrian sedimentation around Ghatshila in east Singhbhum, eastern India. *Proceedings of the National Academy of Sciences, India* **27**, 361–72.
- Naha K** (1965) A critique of “orogenic trends” in Archaean correlation in India. *Tectonophysics* **1**, 431–8.
- Pal DC and Rhede D** (2013) Geochemistry and chemical dating of uraninite in the Jaduguda uranium deposit, Singhbhum shear zone, India: implications for uranium mineralization and geochemical evolution of uraninite. *Economic Geology* **108**, 1499–515.
- Perchuk LL** (1989) Mutual coordination of some Fe-Mg geothermometry on the basis of the Nernst Law: a revision. *Geokhemia* **5**, 611–22.
- Perchuk LL, Aranovich LY, Podlesskii KK, Lavrenteva IV, Gerasimov VY, Fedkin VV, Kitsul VI, Karasakov LP and Berdnikov NV** (1985) Precambrian granulites of the Aldan shield, Eastern Siberia, USSR. *Journal of Metamorphic Geology* **3**, 265–310.
- Perchuk LL and Lavrenteva IV** (1983) Experimental investigation of exchange equilibria in the system cordierite-garnet-biotite. In *Kinetics and Equilibrium in Mineral Reactions* (ed. SK Saxena), pp. 199–239. New York: Springer-Verlag.
- Powell R and Holland TJB** (1988) An internally consistent thermodynamic dataset with uncertainties and correlations: 3. Applications to geobarometry worked examples and a computer program. *Journal of Metamorphic Geology* **6**, 173–204.
- Prakash D, Patel DK, Tewari S, Yadav MK and Yadav R** (2017) Metamorphic zonal sequences of pelitic schists and gneisses from the area around Kandra (Jharkhand): constraints from field and textural relationship. *Journal of the Geological Society of India* **89**, 139–44.
- Ray L, Kumar PS, Reddy GK, Roy S, Rao GV, Srinivasan R and Rao RUM** (2003) High mantle heat flow in a Precambrian granulite province: evidence from southern India. *Journal of Geophysical Research: Solid Earth*, **108**, 2084. doi: 10.1029/2001JB000688.
- Ray S and Gangopadhyay PK** (1971) Metamorphic belts in Singhbhum, Manbhum and Chhota Nagpur, E. India. *Journal of the Geological Society of India* **12**, 286–94.
- Reddy SM, Clarke C and Mazumder R** (2009) Temporal constraints on the evolution of the Singhbhum Crustal Province from U–Pb SHRIMP data. In *Paleoproterozoic Supercontinents and Global Evolution* (eds D Saha and R Mazumder), pp. 17–18. International Association for Gondwana Research, Conference Series 9. Kolkata: Indian Statistical Institute.
- Reddy SM and Evans DAD** (2009) Palaeoproterozoic supercontinents and global evolution: correlations from core to atmosphere. In *Paleoproterozoic Supercontinents and Global Evolution* (eds SM Reddy, R Mazumder, DAD Evans and A Collins), pp. 1–26. Geological Society of London, Special Publication no. 323.
- Robinson D, Reverdatto VV, Bevins RE, Polyansky OP and Sheplev VS** (1999) Thermal modeling of convergent and extensional tectonic settings for the development of low-grade metamorphism in the Welsh Basin. *Journal of Geophysical Research: Solid Earth* **104**, 23069–80.
- Roy A** (1966) The method of continuation in mining geophysical interpretation. *Geoexploration* **4**, 65–83.
- Roy A, Sarkar S, Jeyakumar S, Aggrawal SK and Ebihara M** (2002a) Mid-Proterozoic plume-related thermal event in Eastern Indian craton: evidence from trace elements, REE geochemistry and Sr–Nd isotope systematic of basic-ultrabasic intrusives from Dalma volcanic belt. *Gondwana Research* **5**, 133–46.
- Roy A, Sarkar S, Jeyakumar S, Aggrawal SK and Ebihara M** (2002b) Sm–Nd age and mantle characteristics of the Dhanjori volcanic rocks, Eastern India. *Geochemical Journal* **36**, 503–18.
- Saha AK** (1970) The present status of the Precambrian geology of the Singhbhum region. In *Proceedings of the 2nd Symposium on Upper Mantle Project, 28–31 December, Hyderabad, India*, pp. 259–78. Hyderabad: National Geophysical Research Institute.
- Sarkar AN** (1982) Precambrian tectonic evolution of eastern India: a model of converging microplates. *Tectonophysics* **86**, 363–97.
- Sarkar SN, Ghosh DK and Lambert RJS** (1985) Rubidium–Strontium and lead isotopic studies of the soda granites from Mosabani, Singhbhum copper belt, India. *Indian Journal of Earth Sciences* **13**, 101–16.
- Sarkar SN, Ghosh DK and Lambert RJS** (1986) Rubidium–strontium and lead isotopic studies of the Soda granites from Musaboni area, Singhbhum Copper Belt. In *Geology and Geochemistry of Sulphide Ore Bodies and Associated Rocks in Musaboni and Rakha Mines Section in the Singhbhum Copper Belt* (ed. SN Sarkar), pp. 101–10. Dhanbad: Diamond Jubilee Monograph, Indian School of Mines Dhanbad.
- Sarkar SN and Saha AK** (1962) A revision of the Pre-Cambrian stratigraphy and tectonics of Singhbhum and adjacent regions. *Quarterly Journal of the Geological, Mineralogical and Metallurgical Society of India* **34**, 97–136.
- Sarkar SN and Saha AK** (1977) The present status of the Precambrian stratigraphy, tectonics and geochronology of Singhbhum–Keonjhar–Mayurbhanj region, Eastern India. *Indian Journal of Earth Sciences S. Ray volume*, 37–65.
- Sengupta S and Chattopadhyay B** (2004) Singhbhum mobile belt – how far it fits an ancient orogen. In *Proceedings of the Workshop on (IGCP-453) Uniformitarianism Revised Edition on Orogens of India*, pp. 24–31. Hyderabad: Geological Survey of India, Special Publication no. 84.
- Sengupta S, Sarkar G, Ghosh-Roy AK, Bhaduri SK, Gupta SN and Mandal A** (2000) Geochemistry and Rb–Sr geochronology of acid tuffs from the northern fringe of the Singhbhum craton and their significance in the Precambrian evolution. *Indian Minerals* **54**, 43–56.
- Spear FS** (1993) *Metamorphic Phase Equilibria and Pressure-Temperature-Time Path*. Mineralogical Society of America Monograph. Chelsea, MI: Book Crafters, 799 pp.
- Thompson AB** (1976) Mineral reaction in pelitic rocks: I. Prediction of P–T–X (Fe–Mg) phase relations. *American Journal of Science* **276**, 401–24.
- Tinkham DK and Ghent ED** (2005) Estimating PT conditions of garnet growth with isochemical phase-diagram sections and the problem of effective bulk-composition. *The Canadian Mineralogist* **43**, 35–50.
- Turner FJ** (1968) *Metamorphic Petrology: Mineralogical and Field Aspects*. New York: McGraw-Hill, 403 pp.
- White RW, Powell R and Clarke GL** (2003) Prograde metamorphic assemblage evolution during partial melting of metasedimentary rocks at low pressures: migmatites from Mt Stafford, Central Australia. *Journal of Petrology* **44**, 1937–60.
- White RW, Powell R, Holland JB, Johnson TE and Green ECR** (2014) New mineral activity-composition relations for thermodynamic calculations in metapelitic systems. *Journal of Metamorphic Geology* **32**, 261–86

- White RW, Powell R and Holland TJB** (2001) Calculation of partial melting equilibria in the system Na₂O–CaO–K₂O–FeO–MgO–Al₂O₃–SiO₂–H₂O (NCKFMASH). *Journal of Metamorphic Geology* **19**, 139–53.
- White RW, Powell R and Holland TJB** (2007) Progress relating to calculation of partial melting equilibria for metapelites. *Journal of Metamorphic Geology* **25**, 511–27.
- Windley BF** (1977) Timing of continental growth and emergence. *Nature* **270**, 426–8.
- Zane A, Sassi R and Guidotti CV** (1998) New data on metamorphic chlorite as a petrogenetic indicator mineral, with special regard to greenschist-facies rocks. *The Canadian Mineralogist* **36**, 713–26.